



Observational ozone data over the global oceans and polar regions: The TOAR-II Oceans data set version 2024

Yugo Kanaya¹, Roberto Sommariva^{2,3}, Alfonso Saiz-Lopez⁴, Andrea Mazzeo⁵, Theodore K. Koenig^{6,47},
Kaori Kawana^{1,7}, James E. Johnson^{8,9}, Aurélie Colomb¹⁰, Pierre Tulet¹¹, Suzie Molloy¹², Ian E. Galbally¹³,
5 Rainer Volkamer^{14,15}, Anoop Mahajan¹⁶, John W. Halfacre¹⁷, Paul B. Shepson¹⁸, Julia Schmale¹⁹, Hélène
Angot²⁰, Byron Blomquist^{15,21}, Matthew D. Shupe^{21,15}, Detlev Helmig²², Junsu Gil²³, Meehye Lee²³, Sean
C. Coburn²⁴, Ivan Ortega²⁵, Gao Chen²⁶, James Lee^{27,28}, Kenneth C. Aikin^{15,29}, David D. Parrish³⁰, John
S. Holloway¹⁵, Thomas B. Ryerson²⁹, Ilana B. Pollack^{15, 29}, Eric J. Williams^{15, 29}, Brian M. Lerner³¹,
Andrew J. Weinheimer²⁵, Teresa Campos²⁵, Frank M. Flocke²⁵, J. Ryan Spackman³², Ilann Bourgeois³³,
10 Jeff Peischl²⁹, Chelsea R. Thompson²⁹, Ralf M. Staebler³⁴, Amir A. Aliabadi³⁵, Wanmin Gong³⁴, Roeland
Van Malderen³⁶, Anne M. Thompson³⁷, Ryan M. Stauffer³⁷, Debra E. Kollonige³⁷, Juan Carlos Gómez
Martin³⁸, Masatomo Fujiwara³⁹, Katie Read²⁸, Matthew Rowlinson^{28,17}, Keiichi Sato⁴⁰, Junichi
Kurokawa⁴⁰, Yoko Iwamoto⁴¹, Fumikazu Taketani¹, Hisahiro Takashima^{42,1}, Monica Navarro Comas⁴³,
Marios Panagi⁴⁴, Martin G. Schultz^{45,46}

15

¹Japan Agency for Marine-Earth Science and Technology (JAMSTEC), Yokohama, Kanagawa 2360001, Japan

²School of Geography, Earth and Environmental Sciences, University of Birmingham, Birmingham, UK

³School of Chemistry, University of Leicester, Leicester, UK

20 ⁴Department of Atmospheric Chemistry and Climate, Institute of Physical Chemistry Blas Cabrera, CSIC, Madrid 28006,
Spain

⁵Lancaster Environment Centre, Lancaster University, Lancaster, UK

⁶State Key Joint Laboratory of Environmental Simulation and Pollution Control, BIC-ESAT and IJRC, College of
Environmental Sciences and Engineering, Peking University, Beijing, China

25 ⁷Now at Institute of Chemical Engineering Sciences, Foundation for Research and Technology–Hellas (FORTH/ICE-HT),
Patras, 26504, Greece and School of Architecture, Civil and Environmental Engineering, École Polytechnique Fédérale de
Lausanne (EPFL), Lausanne, 1015, Switzerland

⁸Cooperative Institute for Climate, Ocean, and Ecosystem Studies, University of Washington, Seattle, WA 98105, USA

⁹NOAA Pacific Marine Environmental Laboratory, Seattle, WA 98115, USA

¹⁰LAMP, Laboratoire de Météorologie Physique (UMR 6016 Université Clermont Auvergne, CNRS), Aubière, France

30 ¹¹LAERO, Laboratoire d'Aérodynamique (UMR 5560 CNRS, UT3, IRD), Toulouse, France

¹²Climate, Atmosphere & Ocean Interactions Program, Environment Research Unit, CSIRO, Aspendale, Victoria, Australia

¹³CSIRO Environment, Aspendale, Victoria, Australia

¹⁴Department of Chemistry, University of Colorado, Boulder, CO 80309-0215, USA

¹⁵Cooperative Institute for Research in Environmental Sciences (CIRES), University of Colorado Boulder, Boulder, CO, USA

35 ¹⁶Centre for Climate Change Research, Indian Institute of Tropical Meteorology, Pashan, Pune 411008, India

¹⁷Wolfson Atmospheric Chemistry Laboratories, Department of Chemistry, University of York, York, YO31 7SH, UK

¹⁸School of Marine and Atmospheric Sciences, Stony Brook University, NY 11794-0701, USA

¹⁹Extreme Environments Research Laboratory, École Polytechnique Fédérale de Lausanne, EPFL Valais Wallis, Sion
Switzerland

40 ²⁰Université Grenoble Alpes, CNRS, INRAE, IRD, Grenoble INP, IGE, Grenoble, France

²¹National Oceanic and Atmospheric Administration, Physical Sciences Laboratory, Boulder, CO, USA

²²Boulder A.I.R. LLC, Boulder, Colorado, USA

²³Department of Earth and Environmental Sciences, Korea University, Seoul, Republic of Korea



- 24 Precision Laser Diagnostics Laboratory, University of Colorado Boulder, Boulder, CO, USA
45 25 NSF National Center for Atmospheric Research, ACOM, Boulder, CO 80301, USA
26 NASA Langley Research Center, Hampton, VA 23681, USA
27 Department of Chemistry, University of York, York, UK
28 National Centre for Atmospheric Science, University of York, York, UK
29 NOAA Chemical Sciences Laboratory, Boulder, CO, USA
50 30 David.D.Parrish, LLC, Boulder CO. 80304 USA
31 Aerodyne Research, Inc., Billerica, MA, USA
32 NASA Ames Research Center, Moffett Field, CA 94035, USA
33 Université Savoie Mont Blanc, INRAE, CARRTEL, Thonon-Les-Bains F-74200, France
34 Air Quality Research Division, Science and Technology Branch, Environment and Climate Change Canada, Toronto, Ontario,
55 M3H 5T4, Canada
35 University of Guelph, Guelph, ON, N1G 2W1, Canada
36 Royal Meteorological Institute of Belgium, Ringlaan 3, 1180 Uccle (Brussels), Belgium
37 NASA Goddard Space Flight Center, Greenbelt, MD 20771, USA
38 Instituto de Astrofísica de Andalucía, Consejo Superior de Investigaciones Científicas, 18008, Granada, Spain
60 39 Faculty of Environmental Earth Science, Hokkaido University, Sapporo 060-0810 Japan
40 Asia Center for Air Pollution Research, 1182 Sowa, Nishi-ku, Niigata, Niigata, 950-2144, Japan
41 Graduate School of Integrated Sciences for Life, Hiroshima University, Higashi-Hiroshima, Japan
42 Faculty of Science, Fukuoka University, Fukuoka, Japan
43 Atmospheric Research and Instrumentation Branch, National Institute for Aerospace Technology (INTA), Madrid, Spain
65 44 Climate and Atmosphere Research Center, The Cyprus Institute, 2121, Nicosia, Cyprus
45 Jülich Supercomputing Center, Forschungszentrum Jülich GmbH, 52425 Jülich, Germany
46 Department of Mathematics and Computer Science, University of Cologne, Germany
47 Now at Division of Environment and Sustainability, The Hong Kong University of Science and Technology, Hong Kong
999077, China
70 *Correspondence to:* Yugo Kanaya (yugo@jamstec.go.jp)

Abstract. Studying tropospheric ozone over the remote areas of the planet, such as the open oceans and the polar regions, is crucial to understand the role of ozone as a global climate forcer and regulator of atmospheric oxidative capacity. A focus on the pristine oceanic and polar regions complements the available land-based data sets and provides insights into key photochemical and depositional loss processes that control the concentrations, spatio-temporal variability of ozone, and the physico-chemical mechanisms driving these patterns. However, an assessment of the role of ozone over the oceanic and polar regions has been hampered by a lack of comprehensive observational data sets. Here, we present the first comprehensive collection of ozone data over the oceans and the polar regions. The overall data set consists of 77 ship cruises/buoy-based observations and 48 aircraft-based campaigns. The data set, consisting of more than 630,000 independent ozone measurement data points covering the period from 1977 to 2022 and an altitude range from the surface to 5000 m (with a focus on the lowest 2000 m), allows systematic analyses of the spatio-temporal distribution and long-term trends over the defined 11 ocean/polar regions. The data sets from ships, buoys, and aircrafts are complemented with an ozonesonde data set from 29 launch sites or field campaigns, and by 21 non-polar and 17 polar ground-based stations data sets. The data were filtered by using backward trajectories calculated with the HYSPLIT model from the individual observation points to extract essentially oceanic observations, defined as air masses that have travelled over oceans for 72 hours or more, which were further tested with the



85 coincident Radon observations. The oceanic and polar data thus selected showed typically flat diurnal patterns at high latitudes and daytime decreases (11–16%) at low latitudes, indicating the adequacy of the data collection and processing procedures, as well as the potential for further studies of processes with statistical robustness and coverage. The ship/buoy- and aircraft-based data sets presented here will supplement the land-based ones in the TOAR-II database to provide a fully global assessment of tropospheric ozone.

90 1. Introduction

As a short-lived species with an estimated lifetime of 25.5 ± 2.2 days (Griffiths et al., 2021, Szopa et al., 2021), both global/hemispheric and regional/local aspects need to be emphasized in the assessment of tropospheric ozone. While the spatio-temporal variation over land is primarily important for assessing vegetation and health impacts, its behavior over the oceans is critical when assessing its climate impact as the third most important greenhouse gas (Forster et al., 2021). The role of ozone in maintaining the global oxidative capacity of the atmosphere through the production of the OH radical also requires understanding on a global scale. The overall budget of tropospheric ozone is dominated by the photochemical production and loss terms (Young et al., 2018). The net loss conditions, which are driven by OH/HO₂ radical chemistry in a low NO_x environment and potentially also by understudied halogen chemistry, occur mostly over remote regions, including over the oceans (Galbally et al., 2000; Monks et al., 1998; Stone et al., 2018; Read et al., 2008; Dickerson et al., 1999; Boylan et al., 2015; Saiz-Lopez and von Glasow, 2012; Simpson et al., 2015). Another important loss term is from dry deposition on the ocean surface, which depends on the chemical composition of the surface seawater and its physical conditions (Helmig et al., 2012; Hardacre et al., 2015; Ganzeveld et al., 2009; Pound et al., 2020; Sarwar et al., 2016; Luhar et al., 2018; Barten et al., 2023; Chiu et al., 2024), and which has not been fully characterized. Therefore, there is a special need to study the ozone concentration levels, spatio-temporal variations, and underlying mechanisms that control ozone levels over the oceans. However, observational data of ozone over oceanic regions are much less abundant than those over the land, preventing a full assessment. TOAR (Tropospheric Ozone Assessment Report) is an IGAC (International Global Atmospheric Chemistry project)-sponsored activity which aims to collect ozone observations in the troposphere. At the time of TOAR-I (Schulz et al., 2017), oceanic data were collected only from island-based surface monitoring observations and ozonesondes, with some satellite-based information, but the oceanic regions remained with an apparent void of data.

110 The polar regions in the northern and southern hemispheres are other pristine areas, with episodic ozone destruction in the polar sunrise season (Simpson et al 2007). An assessment report on short-lived climate forcers from the Arctic Council's Arctic Monitoring and Assessment Programme (AMAP, 2021) and synthesis papers (Whaley et al., 2023, Law et al., 2023) have recently been produced, but comprehensive studies based on multi-platform observations are still lacking.

To improve the situation, a working group on ozone over the oceans and the polar regions (Oceans WG) has been formed within the TOAR-II activity to provide a comprehensive data set, especially with ship-, buoy- and aircraft-based observations over the oceans, to allow a first assessment over the entire oceans and polar regions. In the past, studies on O₃ over the oceans



were conducted, using ship-based/aircraft-based O₃ observations, but they were mostly based on observations from a single campaign or a series of related campaigns (e.g., Dickerson et al., 1999, Bourgeois et al., 2020) or at best from a collection of observations from a single nation/project (e.g., Lelieveld et al., 2004, Kanaya et al., 2019); here we aim to collect data from multiple nations, research groups, and campaigns to achieve a better global coverage, using the IGAC framework as a global research network (GRN) of Future Earth on which the TOAR activity is based. The resulting two data sets consist of 77 ship- or buoy-based observations and 48 aircraft observations over the global oceans and polar regions covering a period between 1977 and 2022, and are presented in this data paper. The altitude range covered by the data is from the surface to 5000 m, with a focus on the lowest 2000 m, as a major interest of the WG lies within the atmospheric boundary layer, where the interfacial interactions of the atmosphere with the ocean and snow/ice surfaces (even including biogeochemical processes), as well as the photochemistry, are of particular relevance. A third data set contains ocean and polar ozonesonde data, mostly obtained from coastal/island sonde launching sites. The ozonesonde data were mainly provided by the HEGIFTOM (Harmonization and Evaluation of Ground-based Instruments for Free-Tropospheric Ozone Measurements, <http://hegiftom.meteo.be>) Focus Working Group of the TOAR-II activity and therefore include their data homogenization procedure (Van Malderen et al., 2025), but were further processed by the Oceans WG here. These three data sets are complemented by two data sets containing ground-based data from coastal/island sites and from polar stations, selected from the TOAR-II database (<https://toar-data.org/surface-data/>) with some additional field campaign sites.

The result of this work enables integrated studies of the long-term and/or seasonal trends from ship-based observations and established coastal-site observations in the same region, for example at Cabo Verde and Kennaok-Cape Grim. To be suited for the ocean-focused studies, all five data sets are complemented with information on how many hours each observed air mass was separated from land, derived from backward trajectories. Note that a full assessment of tropospheric ozone in the remote regions (oceans and polar) using these data sets will be published separately (Sommariva et al., in preparation) as part of the TOAR-II series of assessment papers; here we focus on the data description, including its preparation and harmonization.

2 Data description

The overall geographical distribution of the collected ship-buoy data, aircraft-based data (up to 5000 m, but considering 0–2000 m altitude as a key part for the study of the boundary layer), and the locations of the selected ozonesonde/surface observation sites is shown in Fig. 1. The following subsections describe in detail each data set. The data are divided into 11 regions (2 polar and 9 oceanic). Following the recommendation of the TOAR-II Steering Committee (https://igacproject.org/sites/default/files/2023-04/TOAR-II_Community_Special_Issue_Guidelines_202304.pdf), the regions are broadly defined as follows: polar (>60° N and >60° S), mid-latitude (20–60° N and 20–60° S) and tropical (<20° N, <20° S). The boundaries are adjusted by 4 degrees or less to take into account geography or the position of the land masses (Fig. 1). The Pacific sector (from 100–115° E to 100–69° W, across the International Date Line) is subdivided into Northern (R1; 22–63° N), Tropical (R2; 20° S–22° N), and Southern (R3; 20–60° S) regions. The Indian Ocean (from 20–34° E to 100–



115° E) is divided into Tropical (R4; 20° S–31° N) and Southern (R5; 20–60° S) regions. The eastern part of the Mediterranean
150 Sea and the Black Sea (15–55° E, 31–59° N) are given a code R6 but no data are assigned to the region because of the
predominant continental influences. The Atlantic sector (from 100–69° W to 15–20° E) is divided into Northern (R7; from
16–23° N to 62° N), Tropical (R8; 20° S–23° N, including the Caribbean), and Southern (R9; 20–60° S) regions. The Arctic
region (R10) is defined as north of 59–63° N (depending on the longitude) and the Antarctic region (R11) as south of 60° S.

155 2.1 Ship/buoy data set

A total of 208,291 of hourly averaged ozone concentration data were collected from 62 ship cruises (or aggregated
cruises/legs) and from 15 buoy operations and archived in the file `toar2_oceans_ship_buoy_data_250203.csv`, covering the
period 1977–2022 (Table 1). The data come from research groups in the USA, Japan, Australia, Germany, France, Switzerland,
Spain, India, and the Republic of Korea. The instruments used are mainly research-grade ozone monitors based on UV
160 absorption, with the exception of the DWD-MPI data set before 1996 which used a wet chemical instrument using the
potassium iodide (KI) method. The ship’s exhaust plume could affect the observations, depending on the relative wind
directions with respect to the ship’s funnel and the inlet position of the gas sampling tube. A fast response ozone monitor could
easily detect such cases of pollution, as NO in the exhaust titrates the atmospheric ozone quickly. The buoy measurements do
not have the risk of plume effect and therefore their hourly averages were constructed from the original 10-s raw data without
165 filtering to preserve the real O₃ reduction episodes over the Arctic region.

The ship datasets were processed as follows. First, minute data below (hourly mean) - (1 σ) were removed and then hourly
averages were recalculated. The hourly data with minute data where the 1 σ variability is >10% of the hourly mean are then
removed. This two-step filtering procedure is similar to Kanaya et al. (2019) and was found to be suitable to remove the ship’s
influence in different cruise data sets. Figure S1 shows a case of flagging and data removal from the time series of the R/V
170 *Hakuho Maru* cruise KH18-6. Filtering was applied to cruises for which 1-minute based data were available, e.g., Mirai (MR)
12–21, *Hakuho Maru* KH-18-6, NAAMES1–4, ATOMIC, DYNAMO, WACS, VOCALS, NEAQS 2002, NEAQS 2004,
TEXAQS 2006, ICEALOT, CalNex 2010, DRAKE2009, IN MAP-IO (SWINGS 2021, OP1 TAAF 2021, SCRATCH 2021,
OP2 TAAF 2021, MAYOBS 2021, OP3 TAAF 2021, OP4 TAAF 2021; www.mapio.re), *Ka'imimoana*, 17v01-05, 18v01-06,
08, 19v01-03, IIOE2, SOE9, and SOE11. The original data from MAGE92, RITS93, RITS94, ACE1, AEROSOLS99-
175 INDOEX, ACE-Asia were on a 30-min basis, and those from Malaspina, SAGA3, DWD-MPI, YES-AQ, MOSAiC were on
an hourly basis. The 30-min data were averaged to hourly. We assumed that basic quality control has been performed (e.g.,
see Angot et al. (2022) for the MOSAiC data set). The DWD-MPI data are a large compilation of 51 cruises with different
research vessels (*Meteor*; *Polarstern*; *Walther Herwig*; *Anton Dohrn*; *Ymer*; *Academie*) collected by Deutscher Wetterdienst
(DWD) in 1977–1996, 27 cruises with the container ship Berlin Express collected by Max Planck Institute (MPI) in 1995-
180 2002, and one *Meteor* cruise conducted by MPI in 2002, with a clear note that the data have been screened for local influences
of the research vessel itself and of nearby passing ships, and that data in and near harbours and in channels have been removed.



185 Some cruises included additional observations of pollution tracers, i.e., CO, NO, NO₂, and condensation nuclei (CN) with diameters larger than 11–13 nm, and these data are archived together with O₃ (see Table 1 and Table S1 for the observation methods and uncertainties). However, the tracer observations did not cover the entire data set and therefore could not be used uniformly for further systematic screening of air masses influenced by pollution arising from nearby land even if present. It is an essential requirement of oceanic ozone studies to be able to distinguish between air masses representing the remote ocean and those influenced by pollution from nearby land. Therefore, we calculated backward trajectories per hourly data set to add the information of the "last contact with land (LCL, in the unit of hours ago)", as a semi-quantitative index indicating how long the air masses were isolated from a land region with potential pollution before the observations. The land mask data from
190 NASA (https://ldas.gsfc.nasa.gov/gldas/data/0.25deg/landmask_mod44w_025.asc, last accessed: 27 May 2019) with a resolution of 0.25° were used. The high-latitude regions (>65° N or >60° S) were not considered as "land", and the land mask was assumed only up to an altitude of 2500 m, as the pollution effect from land would be minimal at higher altitudes. Backward trajectories were computed with the HYSPLIT version 4 model (Draxler and Rolph, 2013) using GDAS1 (1 × 1°) meteorological fields after December 2004, or the NCEP/NCAR Reanalysis Project product (RP{YEAR}{MONTH}.bgl) files
195 with 2.5° resolution for the earlier period. The starting altitude for ship/buoy observations was set to 500 m and the duration to 120 hours. The first point of land contact was marked to provide the LCL information. An LCL value of 120 h was assigned to the air masses if no land contact occurred for the entire period.

We defined a criterion of LCL ≥ 72 hours (hereafter referred to as LCL72) to identify marine air masses that have been minimally influenced by land. Figure 2 shows examples of the backward trajectories calculated for the MR19-03C cruise
200 between Japan and the Arctic and for the RITS94 cruise from North to South America, respectively. The grey and purple lines represent trajectories for marine and land-influencing air mass cases, respectively. The red lines indicate the cases where the observed O₃ mixing ratio was greater than 50 ppb (polluted).

The LCL72 criterion was evaluated using observed radon concentrations from ACE-1 (Whittlestone et al., 1998), ACE-Asia, ATOMIC, ICEALOT, NAAMES1–4, and WACS shipborne observations as a tracer of land contact (Fig. 3). The median and
205 3rd quartile Radon levels are diminished by almost two thirds when LCL increased from 10 to 80 hours, with a clear drop occurring between 60 and 80 hours since the last contact with land. This provides the basis for a 72 hours LCL threshold identifying marine air masses having little or no influence from land.

Although the discrimination between oceanic and land-influenced air masses is imperfect, largely due to the uncertainties in the trajectory calculations, the agreement between the LCL72 and the Radon <1000 mBq m⁻³ criteria (during the campaigns
210 for which this parameter was available) suggests that it is reasonable to apply the LCL72 flag to all the data treated in this study over the global oceans as the first filter against land influences. In subsequent studies on this oceanic ozone data sets, other filters of land influence can be developed and used to meet the requirements of the type of analysis being undertaken. For example, a more stringent criterion (Radon <100 mBq m⁻³) was used to select baseline data at the Kennaook-Cape Grim station (Chambers et al., 2018). The data that met the LCL72 criterion covered 161,037 hours (77% of the original data set).
215 Note that the data with LCL less than 72 hours is kept in the data file, which may be useful for other purposes.



2.2 Aircraft data

Table 2 lists the 48 airborne campaigns included in the `toar2_oceans_airborne_data_5000m_250203.csv` dataset. The land mask mentioned in Section 2.1 was used to extract the airborne observations over the oceans. The high latitude data ($>65^\circ$ N, or $>60^\circ$ S) were not masked and were used directly. The original merge-type data files from aircraft observations had different time resolutions, from <10 to 90 s; particularly for old missions only a coarse time resolution was available. Considering the temporal coverage and taking advantage of the relatively high temporal resolution of the more recent data, a variable temporal resolution in the range of 10–90 s was used. For campaigns where data with a higher temporal resolution (e.g., 1 Hz) were available, e.g., from FAAM measurements, the data were averaged over 10 s. A total of 424,005 and 252,086 data records for the altitudes <5000 m and <2000 m, respectively, are included in the data set, covering a period from 1987 to 2020. The data came from the US, UK and Germany/Canada, and covered almost all global regions except for the R4 region (tropical Indian Ocean). Data for R5 (southern Indian Ocean) were sparse: only 62 points from the TRACE-A mission. The instruments used for the measurements of ozone are generally based on fast response, e.g., high sensitivity chemiluminescence or UV absorption. Additional data on observations of pollutant tracers, i.e., CO, NO, and NO₂, were archived together (Table S2). The backward trajectories were applied to each measurement point, similar to the ship/buoy-based data, with the starting altitude set to the GPS altitude of the aircraft or to 500 m when it was lower. The proportions of the data meeting the LCL72 criterion were 74% and 63% for the <5000 m and <2000 m cases, respectively.

2.3 Ozonesonde data

A total of 29 selected ozonesondes launch sites/campaigns are included in the `toar2_oceans_ozonesondata_250203.csv` dataset. The sites are listed in Table 3 and shown in Fig. 1. There are no data for regions R4 (Indian Ocean) and R9 (South Atlantic). As the availability of geopotential height information was considered a high priority in the creation of the dataset, data from earlier dates when this parameter was not available (e.g., Alert before 2000) were not included. The ozone mixing ratio was calculated from the atmospheric pressure and the ozone partial pressure data. To reduce the data volume, one data point every 200 m (data closest to the top of each layer, e.g., near to 200 m, 400 m, etc.) was extracted up to the 5000 m altitude. Most of the sites (24 out of 29) were taken from the homogenized HEGIFTOM dataset (<https://hegiftom.meteo.be/datasets/ozonesondes>) to ensure data quality. The selected launch sites are on islands or close to the coast. The other 5 data sources are from island and shipboard campaigns in the tropical Pacific, with the addition of three data sets in R11 (Antarctic region) from the World Ozone and Ultraviolet Radiation Data Centre (WOUDC) ozonesonde database to improve the coverage. The data are all from Electrochemical Concentration Cell (ECC) type ozonesondes. In total, 666,470 and 254,276 data points below 5000 and 2000 m altitude, respectively, were collected.



Backward trajectory calculations were only performed for selected heights (500, 1000, 1500, 2000, 3000, 4000, and 5000 m) to save the computational cost. The LCL information relative to the closest of the height points was used. The proportions of the data meeting the LCL72 criterion were 80% and 67%, for the full data set (<5000 m altitude) and for the <2000 m data subset, respectively. As the launch site is usually on land, the latitude/longitude information from the backward trajectories at 0 and 1 h prior to launch was not included in the LCL calculation. Therefore, the potential influence of local air pollution in the vicinity of the launch site needs to be considered when using these data. For a further characterisation of air masses and screening, wind direction sector information (Table 3), constructed from the coordinates from the backward trajectory files at 0 and 1 hour before launch, was added to the data set.

255 2.4 Non-polar coastal sites data

The list of 21 non-polar coastal sites included in the `toar2_oceans_coastalsites_250203.csv` file is shown in Table 4, and their locations in Fig. 1: 16 sites are from the TOAR-II database (<https://toar-data.org/surface-data/>), 2 are from field campaigns, 2 are from the EANET monitoring network, and 1 is from CSIRO. The sites were selected on the basis of the availability of high-quality data over long periods (typically for >10 years) and for the global coverage. However, no sites matching these criteria could be found for regions R4 and R5 (Indian Ocean). The Kennaook-Cape Grim dataset available on the TOAR-II database was not used, but rather another dataset provided by CSIRO. The latter was an updated version, extended through to the end of 2020, with the years 1982–2017 inclusive being fully QA/QC data on the WMO GAW/BiPM scale. The period 2018–2020 was in the final stages of QA/QC and the fully finalised dataset has subsequently been published on EBAS (link to WDCRG). Further information on the instruments and uncertainties for each site can be found in the TOAR-II database. Obvious zero or negative data have been removed, resulting in a total of 3,650,267 hourly observations being included. The LCL information based on the backward trajectories is included. To save computational cost, only 6 hourly calculations were performed, and the result at the closest data timestamp was used. It should be noted that the risk of the influence from local air pollution is similar to that of the ozonesonde data set. All sites, except Trinidad Head, which can be screened using the local wind direction information (as shown in Table 3), can be considered, as only affected by air masses from essentially clean regions.

2.5 Polar sites data

The list of 17 polar coastal sites included in the `toar2_oceans_polarsites_250203.csv` file is shown in Table 5 and Fig. 1. Except for Alert and Belgrano stations, where the data came from the Canadian data site and from National Institute for Aerospace Technology (INTA), respectively, the 15 data sets are from the TOAR-II database. A total of 3,362,716 hourly observations were included. Similarly to the case of the non-polar coastal sites, the LCL information based on the backward trajectories is included. To save computational cost, only 6 hourly trajectory calculations were performed, and the result at the closest data timestamp was used.



3 Data overview

280 In this section, some basic data analysis and descriptive statistics of the collected data sets is described, for informational purposes. Detailed discussion of the spatio-temporal distribution of tropospheric ozone and its trends over the oceans and polar regions will be presented in the assessment paper (Sommariva et al., in preparation).

3.1 Latitudinal, longitudinal, and vertical transects

285 Figure 4 shows the latitudinal and longitudinal cross sections of the ship/buoy data, after application of the LCL72 filter. The data are grouped into 10 degrees latitudinal and 20 degrees longitudinal bins. The median values in the southern hemisphere are in the range of 15.2–19.1 ppb, while those in the northern hemisphere are in the range of 20.5–34.0 ppb. As expected, a maximum median value was found between 25–55° N, where the ozone is photochemically produced from precursors anthropogenically emitted over the continents and transported over long distances to the open oceans (Fig. 1, see also Kanaya et al., 2019). The latitudinal distribution is flat, with median values in a narrow range of ca. 20–30 ppb. The high episodes (higher than 75 percentiles) are evident from 35–45° N and 120–140° E, suggesting that the effects of Asian pollution remain in the dataset, consistent with the discussion regarding the LCL72 filter.

295 Figure 5 shows the vertical profiles of the combined aircraft and ozonesonde data, after application of the LCL72 filter. The data are grouped into 250 m altitude bins. The general tendency is that the ozone mixing ratio increases with height, except for R7 (Northern Atlantic), where the minimum median values occurred in the 700–950 m altitude layer. In the tropical Atlantic (R8) there is a constant ozone mixing ratio with height from 1950 to 5000 m, differing from the tropical Pacific (R2) and other regional profiles.

3.2 Ship/buoy-based median concentrations and diurnal variation patterns in individual regions (R1–R11)

300 Table 6 summarizes statistics of hourly data from the ship/buoy data set (satisfying LCL72) to compare median concentrations across defined regions (R1–R11) and to investigate features of average diurnal profile (Fig. 6). First, the number of hourly data for individual regions ranged from 3446 (R4) to 61708 (R10), highlighting the advantage of having this large dataset in one place. For R10 (Arctic), 31549 and 7732 hours of data were from O-Buoy and MOSAiC missions. The data sets for the regions R7–R9 (Atlantic), with contributions from the DWD-MPI cruises, were larger than the Pacific (R1–R3). For all regions, the data are almost equally distributed over the time of day. The average diurnal profiles were calculated as follows: the local time for each point was calculated from the time in UTC with longitude shift, and then 25, 50, and 75 percentiles were calculated for each hourly bin per region.

The average of the 24-hour medians showed variability across regions: For the northern midlatitudes, the Pacific and Atlantic were similar (32.9 and 31.6 ppb for R1 and R7, respectively). For the tropics, the Pacific (13.8 ppb, R2) was lower than the



310 Indian Ocean (16.2 ppb, R4) and the Atlantic (20.0 ppb, R8). For the southern mid-latitudes, the values for the Pacific and Indian Oceans were similar (20.1 and 19.7 ppb for R3 and R5, respectively), while the Atlantic was the lowest (15.4 ppb for R9). The R9 value is even lower than that of R8 and close to that of R11 (15.9 ppb, Antarctic). R10 (26.2 ppb) was slightly lower than R1 and R7 (northern mid-latitudes). While the mixing ratios over the tropics are frequently below 15 ppb, for 30%, 50%, and 59% over the Atlantic (R8), Indian (R4), and Pacific (R2) Oceans, respectively, but are very rarely near zero (<1% of observations are less than 3 ppb; Fig. 7). This is in marked contrast to the Arctic (R10) where a secondary distribution peak is found at around zero, while greater mean and median ozone levels are observed and only 18% of mixing ratios are less than 15 ppb. Roughly one third of these are ozone depletion events (ODEs) and 5.9% of total observations are below 3 ppb. This indicates that the mechanism(s) of Arctic ODEs is either inoperative or less efficient in the tropics.

As noted in Section 1, a unique feature of ozone in the marine boundary layer over the remote oceans is net photochemical loss. This must result in afternoon decreases in ozone levels. Indeed, flat diurnal patterns or daytime decreases are evident for the ship/buoy data in most regions (Fig. 6, Table 6). The diurnal profiles of the oceanic data suggest that the data sets collected are representative of the marine atmosphere. More specifically, the three tropical regions R2, R4 and R8 show relatively large daytime decreases. The local time at which the minima were recorded was 15, 16 and 15 h for R2, R4 and R8, respectively (Table 6), while the maxima were recorded at night or in the morning. The amplitude (maximum minus minimum) of the diurnal variation was 1.7, 2.6 and 2.3 ppb, or 12, 16 and 11% of the mean concentration for R2, R4 and R8, respectively. Previous studies from ship observations (Johnson et al., 1990; Thompson et al., 1993; Dickerson et al., 1999; Watanabe et al., 2005) and from coastal site observations (Oltmans, 1981; Nagao et al., 1999; Galbally et al., 2000; Read et al., 2008; Hu et al., 2010) have focused on diurnal variation with daytime decreases and reported amplitudes of 1–7.5 ppb (7–32% of average concentration levels). These studies are mainly from single sites/campaigns for short periods of time. Our dataset will be useful to investigate the characteristics of ozone diurnal variations more comprehensively and with statistical robustness. Contributions from various chemical pathways (e.g. HO_x and halogen cycles) will be discussed by comparison with model simulations in the upcoming assessment paper. We also plan an in-depth analysis of our first observational findings, including the substantial reduction in the tropical Indian Ocean (R4), consistent with Dickerson et al. (1999), and the relatively early onset of daytime destruction for R8 and R2.

335 **3.3 Consistency between the ground-based observations and the ozonesonde observations at the same sites**

At 7 stations (Alert, Ny Alesund, Trinidad Head, Izana, American Samoa, Syowa, and South Pole), both ground-based and ozonesonde observations were recorded. The consistency between the two data sets was checked by comparing ozone measurements at ground level and the ozone sonde data at the lowest altitude (typically around 200 m). At the Izana site, the comparison was made for the 2200–2400 m altitude layer to match the altitude of the ground-based observations (2373 m). Figure 8 shows 3-year and 2-year comparisons at Alert and American Samoa, as an example. The agreement was found for cases of episodic O₃ decreases in the Arctic and for temporal patterns of variation over days and seasons at both sites, demonstrating the internal consistency of the data sets. Using the ground-based and ozonesonde observations in the Arctic



(including Alert) for the year of 2015 as well as ship/buoy/aircraft observations, Gong et al. (2025) discuss the performance of two chemistry-transport models. Reasonable agreement was also found with scatterplots for all 7 sites (Fig. S2), with R^2 values ranging from 0.60 to 0.95 and slopes of bivariate linear fits ranging from 0.94 to 1.38 when sonde values were plotted against surface observations made within one hour of each other. This analysis indicated the high quality of the two datasets.

4 Data availability

The data sets described in this paper are available as five csv files containing all the corresponding metadata information. The files are named as follows:

1. toar2_oceans_ship_buoy_data_250203.csv
2. toar2_oceans_airborne_data_5000m_250203.csv
3. toar2_oceans_ozonesondedata_250203.csv
4. toar2_oceans_coastalsites_250203.csv
5. toar2_oceans_polarsites_250203.csv

The files contain the key metadata information listed in Tables 1–5. The files are available at <https://www.jamstec.go.jp/egcr/e/atmos/observation/toar2oceansdata/index.html> (Kanaya et al., 2025). We plan to create a DOI pointing to the website.

5 Conclusions and outlook

Under the TOAR-II activity, the Oceans Working Group has, for the first time, collected and collated observational ozone data over the open oceans and polar regions on a global scale. When available, additional pollution tracers (CO, NO, NO₂, CN) were also included. All these data sets are stored in five data files classified by platform type, i.e. ship/buoy, aircraft, ozonesondes, non-polar coastal sites and polar sites. Here we describe the data sets and the details of the pre-processing, filtering and flagging procedures, and show basic analyses of spatio-temporal extent, diurnal variation characteristics and internal consistency. Our focus was on the ship/buoy and aircraft observations, which contain a total of 208,291 and 424,005 records, respectively. The aircraft and ozonesonde data covered an altitude range from the surface to 5000 m, allowing a complete assessment of ozone over the oceans and polar regions with a focus on the atmospheric boundary layer (<2000 m). All data sets were supplemented with information on the number of hours that each observed air mass was separated from land, derived from backward trajectories. The selected criterion of 72 hours or more isolation from land, justified by the coincident Radon observations for some selected data sets, allowed the identification of marine air masses. Flat diurnal patterns or diurnal decreases were found after air mass selection, indicating that the collected data sets are representative of the marine atmosphere. Over the tropics, the amplitude of the observed daytime decreases was 11–16%, with the largest decrease observed in the Indian Ocean.



375 Although the observational data have been collected as widely as possible, they are still not sufficiently dense or homogeneous across the defined regions, depending on the purpose of analysis. In order to interpret the data, the sampling bias needs to be assessed using atmospheric chemistry-transport numerical model simulations (e.g., Sekiya et al., 2020). Even if the sampling bias is present, point-by-point comparisons with spatio-temporal matching model simulations will be useful to study the key processes and mechanisms. Seasonality and long-term trends in the oceanic and polar ozone observations will be a focus of discussion in the forthcoming Assessment (Sommariva et al., in preparation).

380 **Author contribution:**

RS, ASL, and YK designed the study and led the data collection, assisted by TKK, AMaz, JEJ, SM, IEG, AMah, GC, WG, JCGM, KR, and MR. YK, FT, IY, HT, KK, JEJ, ASL, AC, PT, SM, IEG, RV, AMah, JS, HA, BB, MDS, DH, JG, ML, SCC, and IO carried out ship observations, collected data, and contributed to their quality control. JWH and PBS led the O-Buoy observations and contributed to their quality control. RV, TKK, JL, DDP, JSH, TBR, IBP, EJW, BML, AJW, TC, FMF, JRS, 385 IB, JP, CRT, RMStae, and AAA conducted aircraft observations, collected data, and contributed to their quality control. RVM, AMT, RMStau, DEK, JCGM, and MF performed ozonesonde observations, managed the data, and contributed to their quality control and homogenization. SM, IEG, WG, KS, JK, and MGS contributed to data collection from coastal/polar sites and analysis. MGS supervised the data collection and handling. MP contributed to data collection from surface sites. KCA and GC managed data and contributed to data curation including quality assurance. KK and TKK performed filtering of the ship-based 390 data and figure generation. AMaz, TKK, KR, MR, IEG, RS, ASL and YK analyzed the dataset and prepared the figures and tables. YK drafted the manuscript and all the co-authors reviewed and contributed to revisions.

Competing interests:

The authors declare that they have no conflict of interest.

395

Acknowledgements

We acknowledge NSF, UCAR/NCAR, NASA, NOAA (PMEL, CSD), ECCO, EANET, JAMSTEC, and NERC for funding and data management. For R/V *Mirai* cruises, we gratefully acknowledge assistance from the Principal Investigators and staff members of all cruises and support from Global Ocean Development Inc. and Nippon Marine Enterprise, Ltd. Authors thanks 400 the IN MAP-IO support team of the OSU-R and OMP for data from the *Marion Dufresne*. Peter Winkler, Marian de Reus, Jos Lelieveld, Jonathan Williams and Horst Fischer are acknowledged for the DWD-MPI dataset. We acknowledge the use of the CSIRO Marine National Facility (<https://ror.org/01mae9353>) in undertaking this research on R/V *Investigator*. The finalised data will be available from the CSIRO Data Access Portal (DAP) with an accompanying DOI. Paty Matrai, Jan Bottenheim, and Bill Simpson are acknowledged for the O-Buoy data. Data collection as part of the international Multidisciplinary drifting 405 Observatory for the Study of Arctic Climate (MOSAic) expedition with the tag MOSAic20192020, with activities supported by Polarstern expedition AWI_PS122_00. The observations during the MOSAic expedition were funded by the US National



Science Foundation (awards OPP 1807496, 1914781, and 1807163), the Swiss National Science Foundation (grant 200021_188478), the Swiss Polar Institute (grant no. DIRCR-2018-004), the Department of Energy Atmospheric System Research Program (DE-SC0019251), and the US National Oceanic and Atmospheric Administration (NOAA) Physical Sciences Laboratory. A subset of data was provided by the Atmospheric Radiation Measurement (ARM) User Facility, a U.S. Department of Energy Office of Science User Facility managed by the Biological and Environmental Research Program. J.S. holds the Ingvar Kamprad chair for extreme environments research, sponsored by Ferring Pharmaceuticals. M.D.S. was supported by the DOE (DE-SC0021341) and NOAA Cooperative Agreement NA22OAR4320151. I.B.P., J.P., C.R.T., I.B., and B.M.L. were supported in part by NOAA Cooperative Agreements NA17OAR4320101 and NA22OAR4320151. The TORERO (Tropical Ocean tRoposphere Exchange of Reactive halogen species and Oxygenated VOC) and CONTRAST (CONvective TRansport of Active Species in the Tropics) projects were funded by the National Science Foundation (AGS-1104104, AGS-1261740). The involvement of the NSF-sponsored Lower Atmospheric Observing Facilities, managed and operated by the National Center for Atmospheric Research (NCAR) Earth Observing Laboratory (EOL) is acknowledged. The FAAM airborne data was obtained using the BAe-146-301 Atmospheric Research Aircraft [ARA] flown by Airtask Ltd and managed by FAAM Airborne Laboratory, jointly operated by UKRI and the University of Leeds. The HEGIFTOM homogenized ozonesonde data are from PIs David Tarasick, Peter von der Gathen, Nis Jepsen, Rigel Kivi, Bryan Johnson, and Terry Deshler. The WOUDC ozonesonde data are from the Finnish Meteorological Institute - National Meteorological Service of Argentina, Australian Bureau of Meteorology, and Japan Meteorological Agency (JMA) retrieved from the WOUDC site (<https://woudc.org/>). The ozonesonde sounding campaign from the research vessel *Shoyomaru* was conducted as part of the project Soundings of Ozone and Water in the Equatorial Region (SOWER) in collaboration with Japan Fisheries Agency. Regarding the data from Kennaook-Cape Grim, Australian Bureau of Meteorology who own and manage the station, and CSIRO for producing the data set are acknowledged. We gratefully acknowledge the NOAA Air Resources Laboratory (ARL) for providing the HYSPLIT transport model (<https://www.arl.noaa.gov/hysplit/>, last access: 23 November 2024). We acknowledge NDACC HEGIFTOM, SHADOZ data (<https://doi.org/10.57721/SHADOZ-V06>). The CONTRAST and TORERO data are from <https://doi.org/10.5065/D6PK0D6N> and <https://doi.org/10.26023/150P-D7CG-310>. This study was supported by the KAKENHI grant no. 21H04933), and by the ArCS (Arctic Challenge for Sustainability; grant no. JPMXD1300000000) and ArCS II (Grant Number JPMXD1420318865) of the Ministry of Education, Culture, Sports, Science, and Technology of Japan.

References

Abbatt, J. P. D., Leaitch, W. R., Aliabadi, A. A., Bertram, A. K., Blanchet, J.-P., Boivin-Rioux, A., Bozem, H., Burkart, J., Chang, R. Y. W., Charette, J., Chaubey, J. P., Christensen, R. J., Cirisan, A., Collins, D. B., Croft, B., Dionne, J., Evans, G. J., Fletcher, C. G., Galí, M., Ghahreman, R., Girard, E., Gong, W., Gosselin, M., Gourdal, M., Hanna, S. J., Hayashida, H., Herber, A. B., Hesaraki, S., Hoor, P., Huang, L., Husserr, R., Irish, V. E., Keita, S. A., Kodros, J. K., Köllner, F., Kolonjari,



- F., Kunkel, D., Ladino, L. A., Law, K., Lévassieur, M., Libois, Q., Liggio, J., Lizotte, M., Macdonald, K. M., Mahmood, R.,
440 Martin, R. V., Mason, R. H., Miller, L. A., Moravek, A., Mortenson, E., Mungall, E. L., Murphy, J. G., Namazi, M., Norman,
A.-L., O'Neill, N. T., Pierce, J. R., Russell, L. M., Schneider, J., Schulz, H., Sharma, S., Si, M., Staebler, R. M., Steiner, N.
S., Thomas, J. L., von Salzen, K., Wentzell, J. J. B., Willis, M. D., Wentworth, G. R., Xu, J.-W., and Yakobi-Hancock, J.
D.: Overview paper: New insights into aerosol and climate in the Arctic, *Atmos. Chem. Phys.*, 19, 2527–2560,
<https://doi.org/10.5194/acp-19-2527-2019>, 2019.
- 445 AMAP, 2021. AMAP Assessment 2021: Impacts of Short-lived Climate Forcers on Arctic Climate, Air Quality, and Human
Health. Arctic Monitoring and Assessment Programme (AMAP), Tromsø, Norway. x + 375pp
- Angot, H., Blomquist, B., Howard, D., Archer, S., Bariteau, L., Beck, I., Boyer, M., Crotwell, M., Helmig, D., Hueber, J.,
Jacobi, H.-W., Jokinen, T., Kulmala, M., Lan, X., Laurila, T., Madronich, M., Neff, D., Petäjä, T., Posman, K., Quéléver, L.,
Shupe, M. D., Vimont, I., Schmale, J.: Year-round trace gas measurements in the central Arctic during the MOSAiC
450 expedition. *Scientific Data*, 9(1), 723, <https://doi.org/10.1038/s41597-022-01769-6>, 2022.
- Barten, J. G.M., Ganzeveld, L. N., Steeneveld, G.-J., Blomquist, B. W., Angot, H., Archer, S. D., Bariteau, L., Beck, I., Boyer,
M., von der Gathen, P., Helmig, D., Howard, D., Hueber, J., Jacobi, H.-W., Jokinen, T., Laurila, T., Posman, K. M., Quéléver,
L., Schmale, J., Shupe, M. D., Krol, M. C.: Low ozone dry deposition rates to sea ice during the MOSAiC field campaign:
Implications for the Arctic boundary layer ozone budget, *Elementa: Science of the Anthropocene*, 11 (1), 00086, doi:
455 <https://doi.org/10.1525/elementa.2022.00086>, 2023.
- Bourgeois, I., Peischl, J., Thompson, C. R., Aikin, K. C., Campos, T., Clark, H., Commane, R., Daube, B., Diskin, G. W.,
Elkins, J. W., Gao, R.-S., Gaudel, A., Hintsä, E. J., Johnson, B. J., Kivi, R., McKain, K., Moore, F. L., Parrish, D. D., Querel,
R., Ray, E., Sánchez, R., Sweeney, C., Tarasick, D. W., Thompson, A. M., Thouret, V., Witte, J. C., Wofsy, S. C., and
Ryerson, T. B.: Global-scale distribution of ozone in the remote troposphere from the ATom and HIPPO airborne field
460 missions, *Atmos. Chem. Phys.*, 20, 10611–10635, <https://doi.org/10.5194/acp-20-10611-2020>, 2020.
- Boylan, P., Helmig, D., Oltmans, S.: Ozone in the Atlantic Ocean marine boundary layer, *Elementa: Science of the
Anthropocene*, 3, 000045, <https://doi.org/10.12952/journal.elementa.000045>, 2015.
- Chambers, S.D., Williams, A.G., Crawford, J., Griffiths, A.D., Krummel, P.B., Steele, L.P., Law, R.M., van der Schoot, M.V.,
Galbally, I.E., Molloy, S.B.: A radon-only technique for characterising “baseline” constituent concentrations at Cape Grim.
465 In: Derek, N., Krummel, P.B., Cleland, S.J. (Eds.), *Baseline Atmospheric Program Australia 2011-2013*. Australian Bureau
of Meteorology and CSIRO Marine and Atmospheric Research, 2018.
- Chiu, R., Obersteiner, F., Franchin, A., Campos, T., Bailey, A., Webster, C., Zahn, A., and Volkamer, R.: Intercomparison of
fast airborne ozone instruments to measure eddy covariance fluxes: spatial variability in deposition at the ocean surface and
evidence for cloud processing, *Atmos. Meas. Tech.*, 17, 5731–5746, <https://doi.org/10.5194/amt-17-5731-2024>, 2024.
- 470 Coburn, S., Ortega, I., Thalman, R., Blomquist, B., Fairall, C. W., and Volkamer, R.: Measurements of diurnal variations and
eddy covariance (EC) fluxes of glyoxal in the tropical marine boundary layer: description of the Fast LED-CE-DOAS
instrument, *Atmos. Meas. Tech.*, 7, 3579–3595, <https://doi.org/10.5194/amt-7-3579-2014>, 2014.



- Dickerson, R. R., Rhoads, K. P., Carsey, T. P., Oltmans, S. J., Burrows, J. P., and Crutzen, P. J.: Ozone in the remote marine boundary layer: A possible role for halogens, *J. Geophys. Res.*, 104(D17), 21385–21395, 475 <https://doi.org/10.1029/1999JD900023>, 1999.
- Draxler, R. R. and Rolph, G. D.: HYSPLIT (HYbrid Single-Particle Lagrangian Integrated Trajectory), NOAA Air Resources Laboratory, College Park, MD, USA, available at: <https://www.arl.noaa.gov/hysplit/hysplit/> (last access: 24 Nov 2024), 2013.
- Fishman, J., Hoell Jr., J. M., Bendura, R. D., McNeal, R. J., Kirchhoff, V. W. J. H.: NASA GTE TRACE A experiment 480 (September–October 1992): Overview, *J. Geophys. Res.*, 101(D19), 23865–23879, <https://doi.org/10.1029/96JD00123>, 1996.
- Forster, P., Storelvmo, T., Armour, K., Collins, W., Dufresne, J.-L., Frame, D., Lunt, D. J., Mauritsen, T., Palmer, M. D., Watanabe, M., Wild, M., and Zhang, H.: The Earth’s Energy Budget, Climate Feedbacks, and Climate Sensitivity. In 485 *Climate Change 2021: The Physical Science Basis. Contribution of Working Group I to the Sixth Assessment Report of the Intergovernmental Panel on Climate Change* [Masson-Delmotte, V., P. Zhai, A. Pirani, S.L. Connors, C. Péan, S. Berger, N. Caud, Y. Chen, L. Goldfarb, M.I. Gomis, M. Huang, K. Leitzell, E. Lonnoy, J.B.R. Matthews, T.K. Maycock, T. Waterfield, O. Yelekçi, R. Yu, and B. Zhou (eds.)]. Cambridge University Press, Cambridge, United Kingdom and New York, NY, USA, pp. 923–1054, <https://doi.org/10.1017/9781009157896.009>, 2021.
- Fujiwara, M., Xie, S.-P., Shiotani, M., Hashizume, H., Hasebe, F., Vömel, H., Oltmans, S. J., Watanabe, T.: Upper- 490 tropospheric inversion and easterly jet in the tropics, *J. Geophys. Res.*, 108 (D24), 2796, <https://doi.org/10.1029/2003JD003928>, 2003.
- Galbally, I. E., Bentley, S. T., and Meyer, C. P.: Mid-latitude marine boundary layer ozone destruction at visible sunrise observed at Cape Grim, Tasmania, 41° S, *Geophys. Res. Lett.*, 27, 3841–3844, <https://doi.org/10.1029/1999GL010943>, 2000.
- Ganzeveld, L., Helmig, D., Fairall, C., Hare, J., and Pozzer, A.: Atmosphere-ocean ozone exchange: A global modeling study 495 of biogeochemical, atmospheric, and waterside turbulence dependencies, *Global Biogeochem. Cy.*, 23, 4, <https://doi.org/10.1029/2008GB003301>, 2009.
- Gómez Martín, J. C., H. Vömel, T. D. Hay, A. S. Mahajan, C. Ordóñez, M. C. Parrondo Sempere, M. Gil-Ojeda, and A. Saiz-Lopez, On the variability of ozone in the equatorial eastern Pacific boundary layer, *J. Geophys. Res. Atmos.*, 121, 11,086– 11,103, <https://doi.org/10.1002/2016JD025392>, 2016.
- 500 Gong, W., Beagley, S. R., Toyota, K., Skov, H., Christensen, J. H., Lupu, A., Pendlebury, D., Zhang, J., Im, U., Kanaya, Y., Saiz-Lopez, A., Sommariva, R., Effertz, P., Halfacre, J. W., Jepsen, N., Kivi, R., Koenig, T. K., Müller, K., Nordström, C., Petropavlovskikh, I., Shepson, P. B., Simpson, W. R., Solberg, S., Staebler, R. M., Tarasick, D. W., Van Malderen, R., and Vestenius, M.: Modelling Arctic Lower Tropospheric Ozone: processes controlling seasonal variations, *EGUsphere* [preprint], <https://doi.org/10.5194/egusphere-2024-3750>, 2025.
- 505 Griffiths, P. T., Murray, L. T., Zeng, G., Shin, Y. M., Abraham, N. L., Archibald, A. T., Deushi, M., Emmons, L. K., Galbally, I. E., Hassler, B., Horowitz, L. W., Keeble, J., Liu, J., Moeini, O., Naik, V., O’Connor, F. M., Oshima, N., Tarasick, D.,



- Tilmes, S., Turnock, S. T., Wild, O., Young, P. J., and Zanis, P.: Tropospheric ozone in CMIP6 simulations, *Atmos. Chem. Phys.*, 21, 4187–4218, <https://doi.org/10.5194/acp-21-4187-2021>, 2021.
- 510 Halfacre, J. W., Knepp, T. N., Shepson, P. B., Thompson, C. R., Pratt, K. A., Li, B., Peterson, P. K., Walsh, S. J., Simpson, W. R., Matrai, P. A., Bottenheim, J. W., Netcheva, S., Perovich, D. K., and Richter, A.: Temporal and spatial characteristics of ozone depletion events from measurements in the Arctic, *Atmos. Chem. Phys.*, 14, 4875–4894, <https://doi.org/10.5194/acp-14-4875-2014>, 2014.
- Hardacre, C., Wild, O., and Emberson, L.: An evaluation of ozone dry deposition in global scale chemistry climate models, *Atmos. Chem. Phys.*, 15, 6419–6436, <https://doi.org/10.5194/acp-15-6419-2015>, 2015.
- 515 Harris, J. M. and Oltmans, S. J.: Variations in tropospheric ozone related to transport at American Samoa, *J. Geophys. Res.*, 102 (D7), 8781–8791, 1997.
- Harriss, R. C., Garstang, M., Wofsy, S. C., Beck, S. M., Bendura, R. J., Coelho, J. R. B., Drewry, J. W., Hoell Jr., J. M., Matson, P. A., McNeal, R. J., Molion, L. C. B., Navarro, R. L., Rabine, V., Snell, R. L.: The Amazon Boundary Layer Experiment: Wet season 1987, *J. Geophys. Res.*, 95(D10), 16721–16736, <https://doi.org/10.1029/JD095iD10p16721>, 1990.
- 520 Harriss, R. C., Wofsy, S. C., Hoell Jr., J. M., Bendura, R. J., Drewry, J. W., McNeal, R. J., Pierce, D., Rabine, V., Snell, R. L.: The Arctic Boundary Layer Expedition (ABLE-3B): July–August 1990, *J. Geophys. Res.*, 99(D1), 1635–1643, <https://doi.org/10.1029/93JD01788>, 1994.
- Harriss, R. C., Wofsy, S. C., Bartlett, D. S., Shipham, M. C., Jacob, D. J., Hoell Jr., J. M., Bendura, R. J., Drewry, J. W., McNeal, R. J., Navarro, R. L., Gidge, R. N., Rabine, V. E.: The Arctic Boundary Layer Expedition (ABLE 3A): July–
- 525 August 1988, *J. Geophys. Res.*, 97(D15), 16383–16394, <https://doi.org/10.1029/91JD02109>, 1992.
- Helmig, D., Lang, E. K., Bariteau, L., Boylan, P., Fairall, C. W., Ganzeveld, L., Hare, J. E., Hueber, J., and Pallandt, M.: Atmosphere-ocean ozone fluxes during the TexAQS 2006, STRATUS 2006, GOMECC 2007, GasEx 2008, and AMMA 2008 cruises, *J. Geophys. Res.-Atmos.*, 117, D4, <https://doi.org/10.1029/2011JD015955>, 2012.
- Hoell Jr., J. M., Davis, D. D., Gregory, G. L., McNeal, R. J., Bendura, R. J., Drewry, J. W., Barrick, J. D., Kirchhoff, V. W.
- 530 J. H., Motta, A. G., Navarro, R. L., Dorko, W. D., Owen, D. W.: Operational overview of the NASA GTE/CITE 3 airborne instrument intercomparisons for sulfur dioxide, hydrogen sulfide, carbonyl sulfide, dimethyl sulfide, and carbon disulfide, *J. Geophys. Res.*, 98(D12), 23291–23304, <https://doi.org/10.1029/93JD00453>, 1993.
- Hoell, J. M., Davis, D. D., Jacob, D. J., Rodgers, M. O., Newell, R. E., Fuelberg, H. E., McNeal, R. J., Raper, J. L., Bendura, R. J.: Pacific Exploratory Mission in the tropical Pacific: PEM-Tropics A, August–September 1996, *J. Geophys. Res.*,
- 535 104(D5), 5567–5583, 1999.
- Hoell, J. M., Davis, D. D., Liu, S. C., Newell, R. E., Akimoto, H., McNeal, R. J., Bendura, R. J.: The Pacific Exploratory Mission–West Phase B: February–March, 1994, *J. Geophys. Res.*, 102(D23), 28223–28239, <https://doi.org/10.1029/97JD02581>, 1997.



- 540 Hoell, J. M., Davis, D. D., Liu, S. C., Newell, R., Shipham, M., Akimoto, H., McNeal, R. J., Bendura, R. J., J. W. Drewry:
Pacific Exploratory Mission–West A (PEM–West A): September–October 1991, *J. Geophys. Res.*, 101(D1), 1641–1653,
<https://doi.org/10.1029/95JD00622>, 1996.
- Hu, X.-M., Sigler, J. M., Fuentes, J. D.: Variability of ozone in the marine boundary layer of the equatorial Pacific Ocean, *J. Atmos. Chem.*, 66, 117–136, 2010.
- 545 Inamdar, S., Tinel, L., Chance, R., Carpenter, L. J., Sabu, P., Chacko, R., Tripathy, S. C., Kerkar, A. U., Sinha, A. K., Bhaskar,
P. V., Sarkar, A., Roy, R., Sherwen, T. T., Cuevas, C., Saiz-Lopez, A., Ram, K., Mahajan, A. S.: Estimation of Reactive
Inorganic Iodine Fluxes in the Indian and Southern Ocean Marine Boundary Layer, *Atmos. Chem. Phys.*, 20, 12093–12114,
<https://doi.org/10.5194/acp-20-12093-2020>, 2020.
- Jacob, D. J., Crawford, J. H., Maring, H., Clarke, A. D., Dibb, J. E., Emmons, L. K., Ferrare, R. A., Hostetler, C. A., Russell,
P. B., Singh, H. B., Thompson, A. M., Shaw, G. E., McCauley, E., Pederson, J. R., and Fisher, J. A.: The Arctic Research
550 of the Composition of the Troposphere from Aircraft and Satellites (ARCTAS) mission: design, execution, and first results,
Atmos. Chem. Phys., 10, 5191–5212, <https://doi.org/10.5194/acp-10-5191-2010>, 2010.
- Jacob, D. J., Crawford, J. H., Kleb, M. M., Connors, V. S., Bendura, R. J., Raper, J. L., Sachse, G. W., Gille, J. C., Emmons,
L., Heald, C. L.: Transport and Chemical Evolution over the Pacific (TRACE-P) aircraft mission: Design, execution, and
first results, *J. Geophys. Res.*, 108 (D20), 9000, <https://doi.org/10.1029/2002JD003276>, 2003.
- 555 Johnson, J. E., Gammon, R. H., Larsen, J., Bates, T. S., Oltmans, S. J., and Farmer, J. C.: Ozone in the marine boundary layer
over the Pacific and Indian Oceans: Latitudinal gradients and diurnal cycles, *J. Geophys. Res.*, 95(D8), 11847–11856,
<https://doi.org/10.1029/JD095iD08p11847>, 1990.
- Kanaya, Y., Miyazaki, K., Taketani, F., Miyakawa, T., Takashima, H., Komazaki, Y., Pan, X., Kato, S., Sudo, K., Sekiya, T.,
Inoue, J., Sato, K., and Oshima, K.: Ozone and carbon monoxide observations over open oceans on R/V *Mirai* from 67° S
560 to 75° N during 2012 to 2017: testing global chemical reanalysis in terms of Arctic processes, low ozone levels at low
latitudes, and pollution transport, *Atmos. Chem. Phys.*, 19, 7233–7254, <https://doi.org/10.5194/acp-19-7233-2019>, 2019.
- Kanaya, Y. et al., Observational ozone data over the global oceans and polar regions: The TOAR-II Oceans data set version
2024, <https://www.jamstec.go.jp/egcr/e/atmos/observation/toar2oceansdata/index.html>, 2024.
- Kleb, M. M., Chen, G., Crawford, J. H., Flocke, F. M., and Brown, C. C.: An overview of measurement comparisons from the
565 INTEX-B/MILAGRO airborne field campaign, *Atmos. Meas. Tech.*, 4, 9–27, <https://doi.org/10.5194/amt-4-9-2011>, 2011.
- Law, K. S., Hjorth, J. L., Pernov, J. B., Whaley, C. H., Skov, H., Collaud Coen, M., Langner, J., Arnold, S. R., Tarasick, D.,
Christensen, J., Deushi, M., Effertz, P., Faluvegi, G., Gauss, M., Im, U., Oshima, N., Petropavlovskikh, I., Plummer, D.,
Tsigaridis, K., Tsyro, S., Solberg, S., Turnock, S. T.: Arctic tropospheric ozone trends, *Geophys. Res. Lett.*, 50,
e2023GL103096, <https://doi.org/10.1029/2023GL103096>, 2023.
- 570 Lelieveld, J., Van Aardenne, J., Fischer, H., De Reus, M., Williams, J., and Winkler, P.: Increasing ozone over the Atlantic
Ocean, *Science*, 304, 1483–1487, 2004.



- Luhar, A. K., Woodhouse, M. T., and Galbally, I. E.: A revised global ozone dry deposition estimate based on a new two-layer parameterisation for air–sea exchange and the multi-year MACC composition reanalysis, *Atmos. Chem. Phys.*, 18, 4329–4348, <https://doi.org/10.5194/acp-18-4329-2018>, 2018.
- 575 Mahajan, A. S., Tinel, L., Sarkar, A., Chance, R., Carpenter, L. J., Hulswar, S., Mali, P., Prakash, S., & Vinayachandran, P. N.: Understanding Iodine Chemistry over the Northern and Equatorial Indian Ocean. *J. Geophys. Res. Atmos.*, 124, 8104–8118, <https://doi.org/10.1029/2018JD029063>, 2019.
- Monks, P.S., Carpenter, L.J., Penkett, S.A., Ayers, G.P., Gillett, R.W., Galbally, I.E., Meyer, C.P., Fundamental ozone photochemistry in the remote marine boundary layer: the SOAPEX experiment, measurement and theory, *Atmos. Environ.*, 580 32, 3647–3664, 1998.
- Nagao, I., Matsumoto, K., Tanaka, H.: Sunrise ozone destruction found in the sub-tropical marine boundary layer, *Geophys. Res. Lett.*, 26 3377–3380, 1999.
- Oltmans, S. J.: Surface ozone measurements in clean air, *J. Geophys. Res.*, 86(C2), 1174–1180, <https://doi.org/10.1029/JC086iC02p01174>, 1981.
- 585 Pan, L., Atlas, E., Salawitch, R., Honomichl, S., Bresch, J., Randel, W., Apel, E., Hornbrook, R., Weinheimer, A., Anderson, D., Andrews, S., Baidar, S., Beaton, S., Campos, T., Carpenter, L., Chen, D., Dix, B., Donets, V., Hall, S., Hanisco, T., Homeyer, C., Huey, L., Jensen, J., Kaser, L., Kinnison, D., Koenig, T., Lamarque, J., Liu, C., Luo, J., Luo, Z., Montzka, D., Nicely, J., Pierce, R., Riemer, D., Robinson, T., Romashkin, P., Saiz-Lopez, A., Schauffler, S., Shieh, O., Stell, M., Ullmann, K., Vaughan, G., Volkamer, R. and Wolfe, G.: The Convective Transport of Active Species in the Tropics (CONTRAST) Experiment, *Bull. Amer. Meteorol. Soc.*, 98(1), 106–128, <https://doi.org/10.1175/BAMS-D-14-00272.1>, 2017.
- Pollack, I. B., Lerner, B. T., and Ryerson, T. B.: Evaluation of ultraviolet light-emitting diodes for detection of atmospheric NO₂ by photolysis-chemiluminescence, *J. Atmos. Chem.*, 65, 111–125, <https://doi.org/10.1007/s10874-011-9184-3>, 2011.
- Pound, R. J., Sherwen, T., Helmig, D., Carpenter, L. J., and Evans, M. J.: Influences of oceanic ozone deposition on tropospheric photochemistry, *Atmos. Chem. Phys.*, 20, 4227–4239, <https://doi.org/10.5194/acp-20-4227-2020>, 2020.
- 595 Prados-Roman, C., Cuevas, C. A., Hay, T., Fernandez, R. P., Mahajan, A. S., Royer, S.-J., Galí, M., Simó, R., Dachs, J., Großmann, K., Kinnison, D. E., Lamarque, J.-F., and Saiz-Lopez, A.: Iodine oxide in the global marine boundary layer, *Atmos. Chem. Phys.*, 15, 583–593, <https://doi.org/10.5194/acp-15-583-2015>, 2015.
- Raper, J. L., Kleb, M. M., Jacob, D. J., Davis, D. D., Newell, R. E., Fuelberg, H. E., Bendura, R. J., Hoell, J. M., McNeal, R. J.: Pacific Exploratory Mission in the Tropical Pacific: PEM-Tropics B, March–April 1999, *J. Geophys. Res.*, 106(D23), 600 32401–32425, <https://doi.org/10.1029/2000JD900833>, 2001.
- Read, K. A., Mahajan, A. S., Carpenter, L. J., Evans, M. J., Faria, B. V. E., Heard, D. E., Hopkins, J. R., Lee, J. D., Moller, S. J., Lewis, A. C., Mendes, L., McQuaid, J. B., Oetjen, H., Saiz-Lopez, A., Pilling, M. J., and Plane, J. M. C.: Extensive halogen mediated ozone destruction over the tropical Atlantic Ocean, *Nature*, 453, 1232–1235, 2008.



- Ryerson, T. B., Buhr, M. P., Frost, G. J., Goldan, P. D., Holloway, J. S., Hübler, G., Jobson, B. T., Kuster, W. C., McKeen, S. A., Parrish, D. D., Roberts, J. M., Sueper, D. T., Trainer, M., Williams, J., Fehsenfeld, F. C.: Emissions lifetimes and ozone formation in power plant plumes, *J. Geophys. Res.*, 103(D17), 22569–22583, <https://doi.org/10.1029/98JD01620>, 1998.
- Saiz-Lopez, A. von Glasow, R.: Reactive halogen chemistry in the troposphere. *Chem. Soc. Rev.*, 41, 6448–6472, 2012.
- Sarwar, G., Kang, D., Foley, K., Schwede, D., and Gantt, B.: Technical note: Examining ozone deposition over seawater, *Atmos. Environ.*, 141, 255–262, <https://doi.org/10.1016/j.atmosenv.2016.06.072>, 2016.
- 610 Sekiya, T., Kanaya, Y., Sudo, K., Taketani, F., Iwamoto, Y., Aita, M. N., Yamamoto, A., and Kawamoto, K.: Global Bromine- and Iodine-Mediated Tropospheric Ozone Loss Estimated Using the CHASER Chemical Transport Model, *Sola*, 16, 220–227, <https://doi.org/10.2151/sola.2020-037>, 2020.
- Shiotani, M., Fujiwara, M., Hasebe, F., Hashizume, H., Vömel, H., Oltmans, S. J., Watanabe, T.: Ozone-sonde observations in the equatorial Eastern Pacific - the Shoyo-maru survey -, *J. Meteorol. Soc. Jpn.*, 80, No. 4B, 897-909, <https://doi.org/10.2151/jmsj.80.897>, 2002.
- 615 Shon, Z.-H., Madronich, S., Song, S.-K., Flocke, F. M., Knapp, D. J., Anderson, R. S., Shetter, R. E., Cantrell, C. A., Hall, S. R., and Tie, X.: Characteristics of the NO-NO₂-O₃ system in different chemical regimes during the MIRAGE-Mex field campaign, *Atmos. Chem. Phys.*, 8, 7153–7164, <https://doi.org/10.5194/acp-8-7153-2008>, 2008.
- Schultz, M. G., Schröder, S., Lyapina, O., Cooper, O. R., Galbally, I., Petropavlovskikh, I., von Schneidmesser, E., Tanimoto, H., Elshorbany, Y., Naja, M., Seguel, R. J., Dauert, U., Eckhardt, P., Feigenspan, S., Fiebig, M., Hjellbrekke, A.-G., Hong, Y.-D., Kjeld, P. C., Koide, H., Lear, G., Tarasick, D., Ueno, M., Wallasch, M., Baumgardner, D., Chuang, M.-T., Gillett, R., Lee, M., Molloy, S., Moolla, R., Wang, T., Sharps, K., Adame, J. A., Ancellet, G., Apadula, F., Artaxo, P., Barlasina, M. E., Bogucka, M., Bonasoni, P., Chang, L., Colomb, A., Cuevas, Agulló, E., Cupeiro, M., Degorska, A., Ding, A., Fröhlich, M., Frolova, M., Gadhavi, H., Gheusi, F., Gilge, S., Gonzalez, M. Y., Gros, V., Hamad, S. H., Helmig, D., Henriques, D., Hermansen, O., Holla, R., Hueber, J., Im, U., Jaffe, D. A., Komala, N., Kubistin, D., Lam, K. -S., Laurila, T., Lee, H., Levy, I., Mazzoleni, C., Mazzoleni, L. R., McClure-Begley, A., Mohamad, M., Murovec, M., Navarro-Comas, M., Nicodim, F., Parrish, D., Read, K. A., Reid, N., Ries, L., Saxena, P., Schwab, J. J., Scorgie, Y., Senik, I., Simmonds, P., Sinha, V., Skorokhod, A. I., Spain, G., Spangl, W., Spoor, R., Springston, S. R., Steer, K., Steinbacher, M., Suharguniyawan, E., Torre, P., Trickl, T., Weili, L., Weller, R., Xiaobin, X., Xue, L., and Zhiqiang, M.: Tropospheric Ozone Assessment Report: Database and metrics data of global surface ozone observations, *Elementa: Science of the Anthropocene*, 5, 1582, <https://doi.org/10.1525/elementa.244>, 2017.
- 620 H., Elshorbany, Y., Naja, M., Seguel, R. J., Dauert, U., Eckhardt, P., Feigenspan, S., Fiebig, M., Hjellbrekke, A.-G., Hong, Y.-D., Kjeld, P. C., Koide, H., Lear, G., Tarasick, D., Ueno, M., Wallasch, M., Baumgardner, D., Chuang, M.-T., Gillett, R., Lee, M., Molloy, S., Moolla, R., Wang, T., Sharps, K., Adame, J. A., Ancellet, G., Apadula, F., Artaxo, P., Barlasina, M. E., Bogucka, M., Bonasoni, P., Chang, L., Colomb, A., Cuevas, Agulló, E., Cupeiro, M., Degorska, A., Ding, A., Fröhlich, M., Frolova, M., Gadhavi, H., Gheusi, F., Gilge, S., Gonzalez, M. Y., Gros, V., Hamad, S. H., Helmig, D., Henriques, D., Hermansen, O., Holla, R., Hueber, J., Im, U., Jaffe, D. A., Komala, N., Kubistin, D., Lam, K. -S., Laurila, T., Lee, H., Levy, I., Mazzoleni, C., Mazzoleni, L. R., McClure-Begley, A., Mohamad, M., Murovec, M., Navarro-Comas, M., Nicodim, F., Parrish, D., Read, K. A., Reid, N., Ries, L., Saxena, P., Schwab, J. J., Scorgie, Y., Senik, I., Simmonds, P., Sinha, V., Skorokhod, A. I., Spain, G., Spangl, W., Spoor, R., Springston, S. R., Steer, K., Steinbacher, M., Suharguniyawan, E., Torre, P., Trickl, T., Weili, L., Weller, R., Xiaobin, X., Xue, L., and Zhiqiang, M.: Tropospheric Ozone Assessment Report: Database and metrics data of global surface ozone observations, *Elementa: Science of the Anthropocene*, 5, 1582, <https://doi.org/10.1525/elementa.244>, 2017.
- 625 Simpson, W. R., von Glasow, R., Riedel, K., Anderson, P., Ariya, P., Bottenheim, J., Burrows, J., Carpenter, L. J., Frieß, U., Goodsite, M. E., Heard, D., Hutterli, M., Jacobi, H.-W., Kaleschke, L., Neff, B., Plane, J., Platt, U., Richter, A., Roscoe, H., Sander, R., Shepson, P., Sodeau, J., Steffen, A., Wagner, T., and Wolff, E.: Halogens and their role in polar boundary-layer ozone depletion, *Atmos. Chem. Phys.*, 7, 4375–4418, <https://doi.org/10.5194/acp-7-4375-2007>, 2007.
- 630 Simpson, W. R., Brown, S. S., Saiz-Lopez, A., Thornton, J. A. and Von Glasow, R.: Tropospheric halogen chemistry: sources, cycling, and impacts, *Chem. Rev.*, 115, 4035–4062, 2015.



- Singh, H. B., Brune, W. H., Crawford, J. H., Flocke, F., and Jacob, D. J.: Chemistry and transport of pollution over the Gulf of Mexico and the Pacific: spring 2006 INTEX-B campaign overview and first results, *Atmos. Chem. Phys.*, 9, 2301–2318, <https://doi.org/10.5194/acp-9-2301-2009>, 2009.
- Singh, H. B., Brune, W. H., Crawford, J. H., Jacob, D. J., and Russell, P. B.: Overview of the summer 2004 Intercontinental Chemical Transport Experiment–North America (INTEX-A), *J. Geophys. Res.*, 111, D24S01, <http://doi.org/10.1029/2006JD007905>, 2006.
- Stone, D., Sherwen, T., Evans, M. J., Vaughan, S., Ingham, T., Whalley, L. K., Edwards, P. M., Read, K. A., Lee, J. D., Moller, S. J., Carpenter, L. J., Lewis, A. C., and Heard, D. E.: Impacts of bromine and iodine chemistry on tropospheric OH and HO₂: comparing observations with box and global model perspectives, *Atmos. Chem. Phys.*, 18, 3541–3561, <https://doi.org/10.5194/acp-18-3541-2018>, 2018.
- Szopa, S., Naik, V., Adhikary, B., Artaxo, P., Berntsen, T., Collins, W. D., Fuzzi, S., Gallardo, L., Kiendler-Scharr, A., Klimont, Z., Liao, H., Unger, N., and Zanis, P.: Short-Lived Climate Forcers. In *Climate Change 2021: The Physical Science Basis. Contribution of Working Group I to the Sixth Assessment Report of the Intergovernmental Panel on Climate Change* [Masson-Delmotte, V., P. Zhai, A. Pirani, S.L. Connors, C. Péan, S. Berger, N. Caud, Y. Chen, L. Goldfarb, M.I. Gomis, M. Huang, K. Leitzell, E. Lonnoy, J.B.R. Matthews, T.K. Maycock, T. Waterfield, O. Yelekçi, R. Yu, and B. Zhou (eds.)]. Cambridge University Press, Cambridge, United Kingdom and New York, NY, USA, pp. 817–922, <https://doi.org/10.1017/9781009157896.008>, 2021.
- Thompson, A. M., Johnson, J. E., Torres, A. L., Bates, T. S., Kelly, L. C., Atlas, E., Greenberg, J. P., Donahue, N. M., Yvon, S. A., Saltzman, E. S., Heikes, B. G., Mosher, B. W., Shashkov, A. A., Yegorov, V. I.: Ozone observations and a model of marine boundary layer photochemistry during SAGA 3, *J. Geophys. Res.*, 98(D9), 16955–16968, <https://doi.org/10.1029/93JD00258>, 1993.
- Tulet, P., Van Baelen, J., Bosser, P., Brioude, J., Colomb, A., Goloub, P., Pazmino, A., Portafaix, T., Ramonet, M., Sellegri, K., Thyssen, M., Gest, L., Marquestaut, N., Mékiès, D., Metzger, J.-M., Athier, G., Blarel, L., Delmotte, M., Despreaires, G., Dournaux, M., Dubois, G., Duflo, V., Lamy, K., Gardes, L., Guillemot, J.-F., Gros, V., Kolasinski, J., Lopez, M., Magand, O., Noury, E., Nunes-Pinharanda, M., Payen, G., Pianezze, J., Picard, D., Picard, O., Prunier, S., Rigaud-Louise, F., Sicard, M., and Torres, B.: MAP-IO: an atmospheric and marine observatory program on board Marion Dufresne over the Southern Ocean, *Earth Syst. Sci. Data*, 16, 3821–3849, <https://doi.org/10.5194/essd-16-3821-2024>, 2024.
- Ueda, S., Iwamoto, Y., Taketani, F., Liu, M., and Matsui, H.: Morphological features and water solubility of iron in aged fine aerosol particles over the Indian Ocean, *Atmos. Chem. Phys.*, 23, 10117–10135, <https://doi.org/10.5194/acp-23-10117-2023>, 2023.
- Van Malderen, R., Thompson, A. M., Kollonige, D. E., Stauffer, R. M., Smit, H. G. J., Maillard Barras, E., Vigouroux, C., Petropavlovskikh, I., Leblanc, T., Thouret, V., Wolff, P., Effertz, P., Tarasick, D. W., Poyraz, D., Ancellet, G., De Backer, M.-R., Evan, S., Flood, V., Frey, M. M., Hannigan, J. W., Hernandez, J. L., Iarlori, M., Johnson, B. J., Jones, N., Kivi, R., Mahieu, E., McConville, G., Müller, K., Nagahama, T., Notholt, J., Piters, A., Prats, N., Querel, R., Smale, D., Steinbrecht,



- W., Strong, K., and Sussmann, R.: Global Ground-based Tropospheric Ozone Measurements: Reference Data and Individual Site Trends (2000–2022) from the TOAR-II/HEGIFTOM Project, EGU sphere [preprint], <https://doi.org/10.5194/egusphere-2024-3736>, 2025.
- 675 Volkamer, R., Baidar, S., Campos, T. L., Coburn, S., DiGangi, J. P., Dix, B., Eloranta, E. W., Koenig, T. K., Morley, B., Ortega, I., Pierce, B. R., Reeves, M., Sinreich, R., Wang, S., Zondlo, M. A., and Romashkin, P. A.: Aircraft measurements of BrO, IO, glyoxal, NO₂, H₂O, O₂–O₂ and aerosol extinction profiles in the tropics: comparison with aircraft-/ship-based in situ and lidar measurements, *Atmos. Meas. Tech.*, 8, 2121–2148, <https://doi.org/10.5194/amt-8-2121-2015>, 2015.
- Watanabe, K., Nojiri, Y., Kariya, S.: Measurements of ozone concentrations on a commercial vessel in the marine boundary layer over the northern North Pacific Ocean, *J. Geophys. Res.*, 110, D11310, <http://doi.org/10.1029/2004JD005514>, 2005.
- 680 Whaley, C. H., Law, K. S., Hjorth, J. L., Skov, H., Arnold, S. R., Langner, J., Pernov, J. B., Bergeron, G., Bourgeois, I., Christensen, J. H., Chien, R.-Y., Deushi, M., Dong, X., Effertz, P., Faluvegi, G., Flanner, M., Fu, J. S., Gauss, M., Huey, G., Im, U., Kivi, R., Marelle, L., Onishi, T., Oshima, N., Petropavlovskikh, I., Peischl, J., Plummer, D. A., Pozzoli, L., Raut, J.-C., Ryerson, T., Skeie, R., Solberg, S., Thomas, M. A., Thompson, C., Tsigaridis, K., Tsyro, S., Turnock, S. T., von
- 685 Salzen, K., and Tarasick, D. W.: Arctic tropospheric ozone: assessment of current knowledge and model performance, *Atmos. Chem. Phys.*, 23, 637–661, <https://doi.org/10.5194/acp-23-637-2023>, 2023.
- Whittlestone, S., Gras, J. L., and Siems, S. T.: Surface air mass origins during the First Aerosol Characterization Experiment (ACE 1), *J. Geophys. Res.*, 103(D13), 16341–16350, 1998.
- Wofsy, S. C., Daube, B. C., Jimenez, R., Kort, E., Pittman, J. V., Park, S., Commane, R., Xiang, B., Santoni, G., Jacob, D.,
- 690 Fisher, J., Pickett-Heaps, C., Wang, H., Wecht, K., Wang, Q.-Q., Stephens, B. B., Shertz, S., Watt, A. S., Romashkin, P., Campos, T., Haggerty, J., Cooper, W. A., Rogers, D., Beaton, S., Hendershot, R., Elkins, J. W., Fahey, D. W., Gao, R. S., Moore, F., Montzka, S. A., Schwarz, J. P., Perring, A. E., Hurst, D., Miller, B. R., Sweeney, C., Oltmans, S., Nance, D., Hints, E., Dutton, G., Watts, L. A., Spackman, J. R., Rosenlof, K. H., Ray, E. A., Hall, B., Zondlo, M. A., Diao, M., Keeling, R., Bent, J., Atlas, E. L., Lueb, R., Mahoney, M. J.: HIPPO Merged 10-second Meteorology, Atmospheric
- 695 Chemistry, and Aerosol Data. Version 1.0. UCAR/NCAR – Earth Observing Laboratory, http://doi.org/10.3334/CDIAC/HIPPO_010 (CDIAC Release 20121129/ NCAR EOL Version 1.0), 2017.
- Wofsy, S. C., Afshar, S., Allen, H. M., Apel, E. C., Asher, E. C., Barletta, B., Bent, J., Bian, H., Biggs, B. C., Blake, D. R., Blake, N., Bourgeois, I., Brock, C. A., Brune, W. H., Budney, J. W., Bui, T. P., Butler, A., Campuzano-Jost, P., Chang, C. S., Chin, M., Commane, R., Correa, G., Crouse, J. D., Cullis, P. D., Daube, B. C., Day, D. A., Dean-Day, J. M., Dibb, J.
- 700 E., DiGangi, J. P., Diskin, G. S., Dollner, M., Elkins, J. W., Erdesz, F., Fiore, A. M., Flynn, C. M., Froyd, K. D., Gesler, D. W., Hall, S. R., Hanisco, T. F., Hannun, R. A., Hills, A. J., Hints, E. J., Hoffman, A., Hornbrook, R. S., Huey, L. G., Hughes, S., Jimenez, J. L., Johnson, B. J., Katich, J. M., Keeling, R. F., Kim, M. J., Kupc, A., Lait, L. R., McKain, K., Mclaughlin, R. J., Meinardi, S., Miller, D. O., Montzka, S. A., Moore, F. L., Morgan, E. J., Murphy, D. M., Murray, L. T., Nault, B. A., Neuman, J. A., Newman, P. A., Nicely, J. M., Pan, X., Paplawsky, W., Peischl, J., Prather, M. J., Price, D. J.,
- 705 Ray, E. A., Reeves, J. M., Richardson, M., Rollins, A. W., Rosenlof, K. H., Ryerson, T. B., Scheuer, E., Schill, G. P.,



- 710 Schroder, J. C., Schwarz, J. P., St.Clair, J. M., Steenrod, S. D., Stephens, B. B., Strode, S. A., Sweeney, C., Tanner, D.,
Teng, A. P., Thames, A. B., Thompson, C. R., Ullmann, K., Veres, P. R., Wagner, N. L., Watt, A., Weber, R., Weinzierl,
B. B., Wennberg, P. O., Williamson, C. J., Wilson, J. C., Wolfe, G. M., Woods, C. T., Zeng, L. H., and Vieznor, N.: ATom:
Merged Atmospheric Chemistry, Trace Gases, and Aerosols, Version 2. ORNL DAAC, Oak Ridge, Tennessee, USA,
<https://doi.org/10.3334/ORNLDAAC/1925>, 2021.
- 715 Young, P. J., Naik, V., Fiore, A. M., Gaudel, A., Guo, J., Lin, M. Y., Neu, J. L., Parrish, D. D., Rieder, H. E., Schnell, J. L.,
Tilmes, S., Wild, O., Zhang, L., Ziemke, J. R., Brandt, J., Delcloo, A., Doherty, R. M., Geels, C., Hegglin, M. I., Hu, L., Im,
U., Kumar, R., Luhar, A., Murray, L., Plummer, D., Rodriguez, J., Saiz-Lopez, A., Schultz, M.G., Woodhouse, M. T. and
Zeng, G.: Tropospheric Ozone Assessment Report: Assessment of global-scale model performance for global and regional
ozone distributions, variability, and trends, *Elem. Sci. Anth.*, 6, p. 10, <https://doi.org/10.1525/elementa.265>, 2018.



Table 1. List of cruise/buoy data contained in the ship/buoy data file.

Label	Cruise	Platform	Resolution	Year	Data number	Ancillary data	Instrument	Uncertainty	PI/Data Manager/WG member worked on the data	Regions	Literature	Data source
S1	MR12: MR12-02	Mirai	1 h	2012	733	CO	Thermo, 49C	1%	Yugo Kanaya	R1	Kanaya et al. (2019)	
S2	MR13: MR13-04, 05, 06, 14-01, 02	Mirai	1 h	2013	2605	CO	Thermo, 49C	1%	Yugo Kanaya	R1,2,4,10	Kanaya et al. (2019)	
S3	MR14: MR14-04, 05, 06	Mirai	1 h	2014	3561	CO	Thermo, 49C	1%	Yugo Kanaya	R1,2,4,10	Kanaya et al. (2019)	
S4	MR15: MR15-03, 04, 05	Mirai	1 h	2015	2374	CO	Thermo, 49C	1%	Yugo Kanaya	R1,2,5,10	Kanaya et al. (2019)	
S5	MR16: MR16-06, 08, 09	Mirai	1 h	2016	2393	CO	Thermo, 49C	1%	Yugo Kanaya	R1,2,3,10,11	Kanaya et al. (2019)	
S6	MR17: MR17-05C, 08	Mirai	1 h	2017	2662	CO	Thermo, 49C	1%	Yugo Kanaya	R1,2,4,10		DOI: 10.17596/0001879, 10.17596/0001881, 10.17596/0001882
S7	MR18: MR18-04, 05C, 06	Mirai	1 h	2018	2567	CO	Thermo, 49C	1%	Yugo Kanaya	R1,2,3,10,11		DOI: 10.17596/0001886, 10.17596/0001887, 10.17596/0001888, 10.17596/0001889, 10.17596/0001976
S8	MR19: MR19-03C, 04	Mirai	1 h	2019	2712	CO	2B, 205	1%	Yugo Kanaya	R1,2,4,5,10,11		DOI: 10.17596/0002077, 10.17596/0002101, 10.17596/0002118
S9	MR20: MR20-E01, 05C, E02, 01	Mirai	1 h	2020	2787	CO	2B, 205	1%	Yugo Kanaya	R1,2,10		DOI: 10.17596/0002152,



												10.17596/0002165, 10.17596/0002191, 10.17596/0002121
S10	MR21: MR21-01, 03, 05C, 06	Mirai	1 h	2021	2990	CO	2B, 205	1%	Yugo Kanaya	R1,2,10		DOI: 10.17596/0002308, 10.17596/0002310, 10.17596/0002331, 10.17596/0002312, 10.17596/0002313
S11	KH-18-6	Hakuho Maru	1 h	2018	527	CO	2B, 205	1%	Yugo Kanaya	R4,5	Ueda et al. (2023)	
S12	NAAMES1	Atlantis	1 h	2015	525	CN	Thermo, 49C	±(2+5%) ppb	James Johnson	R7		https://saga.pmel.noaa.gov/data/
S13	NAAMES2	Atlantis	1 h	2016	529	CN	Thermo, 49C		James Johnson	R7		https://saga.pmel.noaa.gov/data/
S14	NAAMES3	Atlantis	1 h	2017	486	CN	Thermo, 49C		James Johnson	R7		https://saga.pmel.noaa.gov/data/
S15	NAAMES4	Atlantis	1 h	2018	497	CN	Thermo, 49C		James Johnson	R7,8		https://saga.pmel.noaa.gov/data/
S16	ATOMIC	Ronald H. Brown	1 h	2020	695	CN	Thermo, 49C		James Johnson	R8		https://saga.pmel.noaa.gov/data/
S17	DYNAMO	Roger Revelle	1 h	2011	1130	CN	Thermo, 49C		James Johnson	R4,5		https://saga.pmel.noaa.gov/data/
S18	WACS	Knorr	1 h	2014	192	CN	Thermo, 49C		James Johnson	R7		https://saga.pmel.noaa.gov/data/
S19	VOCALS	Ronald H. Brown	1 h	2008	745	CN	TECO 49		James Johnson	R2,3		https://saga.pmel.noaa.gov/data/
S20	MAGE92	R/V John Vickers	1 h	1992	670	CN	Dasibi 1008 AH	N/A	James Johnson	R1,2		https://saga.pmel.noaa.gov/data/
S21	RITS93	R/V Surveyor	1 h	1993	939	CN	Dasibi 1008 AH	N/A	James Johnson	R1,2,3,9,11		https://saga.pmel.noaa.gov/data/
S22	RITS94	R/V Surveyor	1 h	1994	965	CN	Dasibi 1008 AH and	N/A	James Johnson	R1,2,3,9,11		https://saga.pmel.noaa.gov/data/



							TECO 49					
S23	ACE1	Discoverer	1 h	1995	1102	CN	Dasibi 1008 AH and TECO 49	N/A	James Johnson	R1,2,3		https://saga.pmel.noaa.gov/data/
S24	ACEASIA	Ronald H. Brown	1 h	2001	808	CN	Dasibi 1008 AH and TECO 49	N/A	James Johnson	R1		https://saga.pmel.noaa.gov/data/
S25	NEAQS 2002	Ronald H. Brown	1 h	2002	467	NO, NO ₂	Dasibi 1008 AH and TECO 49	±(2% + 1 ppb)	/Kenneth Aikin	R7		https://csl.noaa.gov/projects/neaqs/
S26	NEAQS 2004	Ronald H. Brown	1 h	2004	699	CO, NO, NO ₂	Dasibi 1008 AH and TECO 49	±(2 + 5%) ppb	/Kenneth Aikin	R7		https://csl.noaa.gov/projects/2004/
S27	TEXAQS 2006	Ronald H. Brown	1 h	2006	604	CO, NO, NO ₂	TECO 49c	±(3% + 0.05) ppbv	/Kenneth Aikin	R7		https://csl.noaa.gov/projects/2006/
S28	ICEALOT	Knorr	1 h	2008	726	CO, NO, NO ₂ , CN_13	TECO 49c	±(2% + 0.05) ppbv	Kenneth Aikin and James Johnson	R7,10		https://csl.noaa.gov/groups/csl7/measurements/2008ICEALOT/
S29	CalNex 2010	Atlantis	1 h	2010	473	CO, NO, NO ₂	Thermo Environmental 49c	±(2% + 1) ppb	/Kenneth Aikin	R1		https://csl.noaa.gov/projects/calnex/
S30	MALASPIÑA	Hesperides	1 h	2010	3733	N/A	UV absorption / 2B-205	N/A	Alfonso Saiz-Lopez	R1,2,3,5,7,8,9	Prados-Roman et al. (2015)	
S31	DRAKE2009	Polar Stern	1 h	2009	215	N/A	2B	N/A	//Theodore Koenig	R9		
S32	MAP-IO/SWING 2021	Marion_Dufresne	1 h	2021	938	N/A	HORIBA APOA-370	N/A	Aurélie Colomb, Pierre Tulet	R5	Tulet et al. (2024)	http://www.mapio.re/ https://www.aeris-data.fr/catalogue-mapio/



S3 3	MAP IO/ OP1 TAAF 2021	Marion_ Dufresne	1 h	2021	630	N/A	HORIB A APOA- 370	N/A	Aurélie Colomb, Pierre Tulet	R4,5	Tulet et al. (2024)	http://www.mapio.re/ https://www.aeris-data.fr/catalogue-mapio/
S3 4	MAP IO/ SCRATCH 2021	Marion_ Dufresne	1 h	2021	342	N/A	HORIB A APOA- 370	N/A	Aurélie Colomb, Pierre Tulet	R4,5	Tulet et al. (2024)	http://www.mapio.re/ https://www.aeris-data.fr/catalogue-mapio/
S3 5	MAP IO/ OP2 TAAF 2021	Marion_ Dufresne	1 h	2021	593	N/A	HORIB A APOA- 370	N/A	Aurélie Colomb, Pierre Tulet	R4,5	Tulet et al. (2024)	http://www.mapio.re/ https://www.aeris-data.fr/catalogue-mapio/
S3 6	MAP IO/ MAYOBS 2021	Marion_ Dufresne	1 h	2021	438	N/A	HORIB A APOA- 370	N/A	Aurélie Colomb, Pierre Tulet	R4,5	Tulet et al. (2024)	http://www.mapio.re/ https://www.aeris-data.fr/catalogue-mapio/
S3 7	MAP IO/ OP3 TAAF 2021	Marion_ Dufresne	1 h	2021	600	N/A	HORIB A APOA- 370	N/A	Aurélie Colomb, Pierre Tulet	R5	Tulet et al. (2024)	http://www.mapio.re/ https://www.aeris-data.fr/catalogue-mapio/
S3 8	MAP IO/ OP4 TAAF 2021	Marion_ Dufresne	1 h	2021	549	N/A	HORIB A APOA- 370	N/A	Aurélie Colomb, Pierre Tulet	R4,5	Tulet et al. (2024)	http://www.mapio.re/ https://www.aeris-data.fr/catalogue-mapio/
S3 9	Ka'imimoana	R/V Ka'imimoana	1 h	2012	505	N/A		N/A	Rainer Volkamer, Theodore Koenig	R2,3	Coburn et al. (2014)	https://www.eol.ucar.edu/field_projects/torero
S4 0	DWD-MPI	Meteor; Polarster- n;Walt- her Her	1 h	1977– 2002	103352	N/A	1977-96: a wet chemical instrume	1977- 96: ± 5ppb, 1995-	//Theodore Koenig	R3,5,7, 8,9,10, 11	Lelieveld et al. (2004)	



		wig;Anton_Dohrn;Ymer;Academie Fedorov_(DWD);1977-1996)+Berlin_Express(MPI;1995-2002);Meteor(MPI;2002)					nt using the potassium iodide (KI) method; 1995-2002: Thermo Instrument UV absorption spectrometer; 2002- Thermo Environmental 49 and 49C	2002: 6%± 2ppb, 2002- <5%				
S41	17v01	Investigator	1 h	2017	1067	N/A	Thermo Scientific 49i analyser ×2	2.3–2.9%	Suzie Molloy	R3,11		https://data.csiro.au/ (Data will be available in 2025)
S42	17v02	Investigator	1 h	2017	223	N/A	Thermo Scientific 49i analyser ×2		Suzie Molloy	R3		
S43	17v03	Investigator	1 h	2017	729	N/A	Thermo Scientific 49i analyser ×2		Suzie Molloy	R3		
S44	17v04	Investigator	1 h	2017	412	N/A	Thermo Scientific 49i analyser ×2		Suzie Molloy	R3		
S45	17v05	Investigator	1 h	2017	670	N/A	Thermo Scientific 49i analyser ×2		Suzie Molloy	R3		
S46	18v01	Investigator	1 h	2018	864	N/A	Thermo Scientific 49i analyser ×2		Suzie Molloy	R2,3,5		



S47	18v02	Investigator	1 h	2018	359	N/A	Thermo Scientific 49i analyser ×2		Suzie Molloy	R3,11		
S48	18v03	Investigator	1 h	2018	397	N/A	Thermo Scientific 49i analyser ×2		Suzie Molloy	R3		
S49	18v04	Investigator	1 h	2018	588	N/A	Thermo Scientific 49i analyser ×2		Suzie Molloy	R3		
S50	18v05	Investigator	1 h	2018	657	N/A	Thermo Scientific 49i analyser ×2		Suzie Molloy	R3		
S51	18v06	Investigator	1 h	2018	581	N/A	Thermo Scientific 49i analyser ×2		Suzie Molloy	R3		
S52	18v08	Investigator	1 h	2018	284	N/A	Thermo Scientific 49i analyser ×2		Suzie Molloy	R3		
S53	19v01	Investigator	1 h	2019	848	N/A	Thermo Scientific 49i analyser ×2		Suzie Molloy	R3,11		
S54	19v02	Investigator	1 h	2019	425	N/A	Thermo Scientific 49i analyser ×2		Suzie Molloy	R3		
S55	19v03	Investigator	1 h	2019	667	N/A	Thermo Scientific 49i analyser ×2		Suzie Molloy	R2,3,5		
S56	IIOE2	R/V Sagar Nidhi	1 h	2015	211	N/A	Ecotech EC9810 B	1 ppbv	Anoop Mahajan	R4,5	Mahajan et al. (2019), Inamdar et al (2020)	
S57	SOE9	S A Agulhas	1 h	2016	1121	N/A	Ecotech EC9810 B	1 ppbv	Anoop Mahajan	R5,11		



S58	SOE11	S A Agulhas	1 h	2020	824	N/A	Ecotech EC9810 B	1 ppbv	Anoop Mahajan	R5,11		
B1	O-Buoy01	O-Buoy	1 h	2009–2010	4741	N/A	custom-built 2B Technologies, model 205 dual-beam O3 monitors	a manufacturer specified limit of detection of 1 nmol mol ⁻¹ , and individual measurement uncertainty was calculated to range from 2.1 to 3.5 nmol mol ⁻¹	John W Halfacre	R10	Halfacre et al. (2014)	
B2	O-Buoy02	O-Buoy	1 h	2010–2011	2832	N/A			John W Halfacre	R10		
B3	O-Buoy03	O-Buoy	1 h	2010–2011	1405	N/A			John W Halfacre	R10		
B4	O-Buoy04	O-Buoy	1 h	2010–2012	4424	N/A			John W Halfacre	R10		
B5	O-Buoy05	O-Buoy	1 h	2011–2012	1036	N/A			John W Halfacre	R10		
B6	O-Buoy06	O-Buoy	1 h	2012	338	N/A			John W Halfacre	R10		
B7	O-Buoy07	O-Buoy	1 h	2012–2013	955	N/A			John W Halfacre	R10		
B8	O-Buoy08	O-Buoy	1 h	2012–2016	2823	N/A			John W Halfacre	R10		



B9	O-Buoy09	O-Buoy	1 h	2013	46	N/A			John W Halfacre	R10		
B10	O-Buoy10	O-Buoy	1 h	2013–2014	3777	N/A			John W Halfacre	R10		
B11	O-Buoy11	O-Buoy	1 h	2014–2015	3338	N/A			John W Halfacre	R10		
B12	O-Buoy12	O-Buoy	1 h	2014–2015	851	N/A			John W Halfacre	R10		
B13	O-Buoy13	O-Buoy	1 h	2015–2016	1881	N/A			John W Halfacre	R10		
B14	O-Buoy14	O-Buoy	1 h	2015–2017	6229	N/A			John W Halfacre	R10		
B15	O-Buoy15	O-Buoy	1 h	2015–2016	389	N/A			John W Halfacre	R10		
S59	YES-AQ	R/V Gisang1	1 h	2015–2021	2156	N/A	Thermo, Model 49C	1 ppb	Junsu Gil	R1		
S60	MOSAiC	R/V Polarstern	1 h	2019–2020	8131	CO	Thermo Fisher Scientific 49i/49c, 2B Technologies 205	manufacturer-specified precisions of 1.0 ppb for 20-s averages, CO 1.5 ppb (5 min)	Julia Schmale	R10	Angot et al. (2022)	https://doi.org/10.1594/PANGAEA.944393 https://doi.org/10.1594/PANGAEA.944389
S61	SAGA3	R/V Korolev	1 h	1990	562	N/A	Dasibimodel 1008-AH	± 3 ppbv	James Johnson	R8	Thompson et al. (1993)	https://saga.pmel.noaa.gov/data/
S62	AEROSOLS99-INDOEX	Ronald H. Brown	1 h	1999	1392	CN	Dasibi 1008 AH and TECO 49	N/A	James Johnson	R4,5,7,8,9		https://saga.pmel.noaa.gov/data/



Table 2. List of aircraft-based campaign data contained in the aircraft data set.

720

Label	Campaign	Platform	Resolution	Year	Data number <2000 m	Data number <5000 m	Ancillary data	Instrument	Uncertainty	PI/Data Manager/WG member worked on the data	Regions	Literature	Data source
A1	ABLE-2B	Electra	60 s	1987	67	677	CO	N/A	N/A	/Gao Chen	R7,8	Harriss et al. (1990)	https://www-gte.larc.nasa.gov/gte_mrg1.htm#ABLE-2B
A2	ABLE-3A	Electra	60 s	1988	1668	3824	NO	N/A	2 ppbv (detection limit)	/Gao Chen	R1,7,10	Harriss et al. (1992)	https://www-gte.larc.nasa.gov/gte_mrg1.htm#ABLE-3A
A3	ABLE-3B	Electra	90 s	1990	133	258	CO, NO, NO ₂	N/A	N/A	/Gao Chen	R7,10	Harriss et al. (1994)	https://www-gte.larc.nasa.gov/gte_mrg1.htm#ABLE-3B
A4	CITE-3	Electra	10 s	1989	21355	28718	CO	chemiluminescence	N/A	/Gao Chen	R7,8	Hoell Jr. et al. (1993)	https://www-gte.larc.nasa.gov/gte_mrg1.htm#CITE-3
A5	PEM-West A	DC-8	90 s	1991	801	1511	CO, NO, NO ₂	Chemiluminescence	5% or 2ppb	/Gao Chen	R1,2	Hoell et al. (1996)	https://www-gte.larc.nasa.gov/gte_mrg1.htm#PEM%20WEST-A
A6	PEM-West B	DC-8	30 s	1994	2142	5259	CO, NO	Chemiluminescence	3% or 2ppb	/Gao Chen	R1,2	Hoell et al. (1997)	https://www-gte.larc.nasa.gov/gte_mrg1.htm#PEM%20WEST-B
A7	TRACE-A	DC-8	90 s	1992	131	408	CO, NO, NO ₂	N/A	N/A	/Gao Chen	R5,7,8,9	Fishman et al. (1996)	https://www-gte.larc.nasa.gov/gte_mrg1.htm#TRACE-A
A8	PEM-Tropics A	DC-8	60 s	1996	1395	2969	CO, NO, NO ₂	Chemiluminescence	3% or 2ppb	/Gao Chen	R1,2,3,11	Hoell et al. (1999)	https://www-gte.larc.nasa.gov/gte_mrg1.htm#PEM%20TROPICS-A
A9	PEM-Tropics B P3B	P3B	60 s	1999	3111	4939	CO, NO, NO ₂	Chemiluminescence	3% or 2ppb	/Gao Chen	R1,2,3,7	Raper et al. (2001)	https://www-gte.larc.nasa.gov/gte_mrg1.htm#PEM%



													20TROPICS-B
A10	PEM-Tropics B DC8	DC-8	60 s	1999	1573	3027	CO, NO, NO ₂	Chemiluminescence	3% or 2ppb	/Gao Chen	R1,2,3,8		
A11	TRACE-P P3B	P3B	60 s	2001	3036	6374	CO, NO, NO ₂	Chemiluminescence	5% or 2 ppb	/Gao Chen	R1,2,7	Jacob et al. (2003)	https://www-gte.larc.nasa.gov/gte_mrg1.htm#TRACE-P
A12	TRACE-P DC8	DC-8	60 s	2001	2024	3925	CO, NO, NO ₂	Chemiluminescence	5% or 2 ppb	/Gao Chen	R1,2	Singh et al. (2006)	
A13	INTEX-NA	DC-8	60 s	2004	1056	1739	CO, NO, NO ₂	Chemiluminescence	5% or 1 ppb	/Gao Chen	R1,7		https://www-air.larc.nasa.gov/missions/intexna/intexna.htm
A14	INTEX-B DC8	DC-8	60 s	2006	1262	2695	CO, NO, NO ₂	Chemiluminescence	1 ppb or 5%	/Gao Chen	R1,2,7	Singh et al. (2009)	https://www-air.larc.nasa.gov/missions/intexb/intexb.html
A15	INTEX-B C-130	C-130	60 s	2006	741	2468	CO, NO, NO ₂	Chemiluminescence	0.1 ppbv or 5%	/Gao Chen	R1,2,7	Shon et al. (2008) , Kleb et al. (2011)	https://www.eol.ucar.edu/field_projects/milagro
A16	ARCTAS	DC-8	60 s	2008	1287	2444	CO, NO, NO ₂	Chemiluminescence	±2 ppbv	Andrew Weinheimer, Denise Montska, David Knapp, and Ilana Pollack	R1,10	Jacob et al. (2010)	https://www-air.larc.nasa.gov/cgi-bin/ArcView/arctas
A17	SEAC4RS DC8	DC-8	60 s	2013	376	601	CO, NO, NO ₂	chemiluminescence	0.030 ppbv + 3%	Tom Ryerson, Jeff Peischl and Ilana Pollack	R1,7		https://www-air.larc.nasa.gov/cgi-bin/ArcView/seac4rs
A18	SEAC4RS ER2	ER2	60 s	2013	83	202	CO	UV absorption	3% ± precision	/Gao Chen	R7		https://www-air.larc.nasa.gov/cgi-bin/ArcView/seac4rs
A19	DISCOVER-AQ	P3B	60 s	2013	145	162	NO, NO ₂	4ch chemiluminescence	0.1 ppbv + 5%	/Gao Chen	R1		https://www-air.larc.nasa.gov/cgi-bin/ArcView/



													discover-aq.co-2014?P3B=1
A20	KORUS-AQ	DC-8	60 s	2016	2057	2631	CO, NO, NO ₂	4ch chemiluminescence,	5 ppbv + 10%	/Gao Chen	R1		https://www-air.larc.nasa.gov/cgi-bin/ArcView/korusaq
A21	ATom1-4	DC-8	10 s	2016 – 2018	23715	42975	CO, NO, NO ₂	4ch chemiluminescence	5-10 ppt	Ilann Bourgeois, Jeff Peischl, Chelsea Thompson	R1,2,3,7,8,9,10,11	Wofsy et al. (2021)	https://daac.ornl.gov/cgi-bin/dsviewer.pl?ds_id=1581
A22	HIPPO	NSF NCAR G- V	10 s	2009 – 2011	20509	45018	CO	Ultraviolet absorption	Final data. Accuracy approximately ±5%	Fahey, Gao, Spackman	R1,2,3,7,8,10,11	Bourgeois et al. (2020) Wofsy et al. (2017)	https://www.eol.ucar.edu/field_projects/hippo
A23	ACSIS FAAM	FAAM/BAE-146-301	10 s	2017 – 2020	23046	34840	CO	TECO 49	N/A	James Lee	R7,8		https://catalogue.ceda.ac.uk/uuid/8df2e81dbfc2499983aa87781fb3fd5a/ https://www.faam.ac.uk/spinx/coredata/dynamic_content/modules.html#teiozone
A24	ACCACIA FAAM	FAAM/BAE-146-301	10 s	2013	7548	11369	CO			James Lee	R10		
A25	CAST FAAM	FAAM/BAE-146-301	10 s	2014	7210	10566	CO			James Lee	R1		
A26	CLARIFY FAAM	FAAM/BAE-146-301	10 s	2017	14248	24319	CO			James Lee	R8		
A27	ITOP FAAM	FAAM/BAE-146-301	10 s	2004	4683	13350	CO			James Lee	R7		
A28	VOCALS FAAM	FAAM/BAE-146-301	10 s	2008	19037	19736	CO			James Lee	R2,3		
A29	NARE1996	NOAA P-3	10 s	1996	3006	4783	CO, NO, NO ₂	N/A	N/A	/Kenneth Aikin	R7		



A30	NARE1997	NOAA P-3	10 s	1997	4886	9931	CO, NO, NO ₂	N/A	N/A	/Kenneth Aikin	R7		
A31	TEXAQS 2000	NCAR Electra	10 s	2000	2496	3904	CO, NO, NO ₂	chemiluminescence	N/A	/Kenneth Aikin	R7	Ryerson et al. (1998)	https://csl.noaa.gov/projects/texaqs2k/
A32	ITCT2002	NOAA WP-3D	10 s	2002	6004	13772	CO, NO, NO ₂	chemiluminescence	±2%	/Kenneth Aikin	R1,7		https://csl.noaa.gov/projects/itct/2k2/
A33	ITCT2004	NOAA WP-3D	10 s	2004	15213	19791	CO, NO, NO ₂	Chemiluminescence	0.1 + 3%)	/Kenneth Aikin	R7		https://csl.noaa.gov/projects/2004/
A34	HURRICANE2006	NOAA G-4	10 s	2006	334	663	none	N/A		/Kenneth Aikin	R7,8		https://csl.noaa.gov/groups/csl7/measurements/2006Hurricane/
A35	TEXAQS 2006	NOAA WP-3D	10 s	2006	5395	6772	CO, NO, NO ₂	Chemiluminescence	0.050 ppbv + 3%	/Kenneth Aikin	R7		https://csl.noaa.gov/projects/2006/
A36	ARCPAC 2008	NOAA WP-3D	10 s	2008	4878	11563	CO, NO, NO ₂	Chemiluminescence	0.05 + 4%	/Kenneth Aikin	R10		https://csl.noaa.gov/projects/arcpac/
A37	CalNex2010	NOAA WP-3D	10 s	2010	7040	9265	CO, NO, NO ₂	Chemiluminescence	0.015 ppbv + 2%	/Kenneth Aikin	R1,7	Pollack et al. (2010)	https://csl.noaa.gov/projects/calnex/
A38	WINTER STORMS 2001	NA	10 s	2001	164	895	none	N/A	N/A	/Kenneth Aikin	R1		
A39	WINTER STORMS 2002	NA	10 s	2002	815	1867	none	N/A	N/A	/Kenneth Aikin	R1,7		
A40	WINTER STORMS 2003	NOAA G-4	10 s	2003	657	2225	none	N/A	N/A	/Kenneth Aikin	R1,7		https://csl.noaa.gov/groups/csl7/measurements/2003WinterStorms/
A41	WINTER STORMS 2004	NOAA G-4	10 s	2004	992	3283	none	N/A	N/A	/Kenneth Aikin	R1,2,7		https://csl.noaa.gov/groups/csl7/measurements/2004WinterStorms/
A42	WINTER STORMS 2005	NOAA G-4	10 s	2005	541	2099	none	N/A	N/A	/Kenneth Aikin	R1		https://csl.noaa.gov/groups/csl7/measurements/2005WinterStorms/
A43	WINTER STORMS 2006	NOAA G-4	10 s	2006	900	1633	none	N/A	N/A	/Kenneth Aikin	R1		https://csl.noaa.gov/groups/csl7/measurements/2006WinterStorms/



A4 4	WINTER STORMS 2007	NOAA G-4	10 s	2007	355	1375	none	N/A	N/A	/Kenneth Aikin	R1,7		https://csl.noaa.gov/groups/csl7/measurements/2007WinterStorms/
A4 5	ACTIVA TE	Falcon	60 s	2020	5983	6797	CO	UV absorption	greater of ±5 ppbv or ±5%	/Gao Chen	R7		https://www-air.larc.nasa.gov/cgi-bin/ArcView/activate.2022?HU25=1
A4 6	CONTRA ST	NSF NCAR G-V	10 s	2014	3308	6318	CO, NO, NO ₂	Chemil umines cence	N/A	Rainer Volkamer	R1,2	Pan et al. (2017)	https://www.eol.ucar.edu/field_projects/contrast
A4 7	TORERO	NSF NCAR G-V	10 s	2012	7129	12569	CO	O3 Dual- channe l UV absorption spectro meter	3% + precision	Rainer Volkamer	R2,3,8	Volkam er et al. (2015)	https://www.eol.ucar.edu/field_projects/torero
A4 8	NETCAR E	Polar 6	10 s	2014 – 2015	17551	27496	none	Therm o Scienti fic Model 49i	N/A	Ralf Staebler	R10	<u>Abbatt et al. (2019)</u>	https://open.canada.ca/data/en/dataset/1143472d-6c73-4b5c-bc2b-a3d5319961e9 https://open.canada.ca/data/en/dataset/ef0e41c-890d-404d-bb1b-421456022d51



Table 3. List of ozonesonde data contained in the ozonesonde data file.

Label	Station	Latitude	Longitude	Year begin	Year end	Data number	GPS lat/lon	GPS altitude	Wind directions for oceanic air masses (see footnote)	Regions	Literature	Data source
O1	Alert	82.50	-62.33	2000	2020	23211	N/A	N/A	all wind directions	R10		HEGIFTOM_homogenized
O2	Eureka	79.99	-85.94	2000	2021	33473	N/A	N/A	all wind directions	R10		HEGIFTOM_homogenized
O3	Resolute	74.71	-94.97	2000	2021	19146	N/A	N/A	all wind directions	R10		HEGIFTOM_homogenized
O4	Scoresbysund	70.48	-21.95	1989	2022	38362	N/A	N/A	all wind directions	R10		HEGIFTOM_homogenized
O5	Sodankyla	67.36	26.62	1994	2022	35893	N/A	N/A	all wind directions	R10		HEGIFTOM_homogenized
O6	Trinidad Head	41.06	-124.15	1997	2021	31441	available	partly available	5, 6 or 7	R1		HEGIFTOM_homogenized
O7	Wallops Island	37.90	-75.70	1995	2020	36700	available	partly available	2, 3 or 4	R7	Witte et al., (2019)	HEGIFTOM_homogenized
O8	Izana	28.46	-16.26	1995	2022	35025	N/A	N/A	all wind directions	R7		HEGIFTOM_homogenized
O9	Hanoi	21.02	105.80	2004	2018	6537	available	partly available		R2		HEGIFTOM_homogenized
O10	Hilo	19.72	-155.05	1982	2021	39389	N/A	partly available	all wind directions	R2		HEGIFTOM_homogenized
O11	Costa Rica	9.98	-84.21	2005	2020	10920	available	partly available		R8		HEGIFTOM_homogenized
O12	Paramaribo	5.81	-55.21	1999	2021	20597	available	partly available	0, 1, 2, 5, 6 or 7	R8		HEGIFTOM_homogenized
O13	Kuala Lumpur	2.73	101.70	1998	2019	10985	available	partly available		R2		HEGIFTOM_homogenized
O14	San Cristobal	-0.92	-89.60	1998	2016	10405	available	partly available	all wind directions	R2		HEGIFTOM_homogenized
O15	Natal	-5.40	-35.40	1998	2019	17505	available	N/A	all wind directions	R8		HEGIFTOM_homogenized
O16	Watukosek	-7.60	112.70	1998	2013	8404	N/A	N/A		R2		HEGIFTOM_homogenized
O17	Ascension Island	-7.56	-14.22	1998	2020	18238	available	partly available	all wind directions	R8		HEGIFTOM_homogenized



O18	Samoa	-14.33	-170.71	1986	2021	25066	N/A	partly available	all wind directions	R2		HEGIFTOM_homogenized
O19	Suva_Fiji	-18.15	178.45	1997	2021	11779	available	partly available	all wind directions	R2		HEGIFTOM_homogenized
O20	Reunion	-21.10	55.50	1998	2020	18470	available	N/A	all wind directions	R5		HEGIFTOM_homogenized
O21	McMurdo	-78.85	166.67	1986	2010	20440	N/A	N/A	all wind directions	R11		HEGIFTOM_homogenized
O22	South Pole	-90.00	-169.00	1967	2021	24122	available	partly available	all wind directions	R11		HEGIFTOM_homogenized
O23	Isabela-San Cristobal	-0.96, -0.92	-90.97, -89.6	2011	2011	400	N/A	N/A	all wind directions	R2	Gómez Martín et al. (2016)	Campaign (ECC)
O24	Lauder	-45.04	169.68	1986	2021	44796	N/A	N/A		R3		HEGIFTOM_homogenized
O25	NyAlesund	78.93	11.95	1992	2022	63633	partly Y	N/A	all wind directions	R10		HEGIFTOM_homogenized
O26	Shoyomaru	variable, see data	variable, see data	1999	1999	350	N/A	N/A	all wind directions	R2	Shiota ni et al. (2002), Fujiwara et al. (2003)	Campaign (ECC)
O27	Marambio	-64.23	-56.62	1988	2019	28057	N/A	N/A	all wind directions	R11		WOUDC (ECC)
O28	Davis	-68.58	77.97	2006	2023	16201	N/A	N/A	all wind directions	R11		WOUDC (ECC)
O29	Syowa	-69.01	39.58	2010	2023	16925	N/A	N/A	all wind directions	R11		WOUDC (ECC only)

725 Note: wind direction codes are [0=N, 1=NE, 2=E, ..., and 7=NW]. Recommendations for Trinidad Head, Wallops Island, and Paramaribo was provisionally included.



730

Table 4. List of non-polar ground-based observations contained in the coastal sites data set.

Label	Station	Latitude	Longitude	Altitude (m)	Year begin	Year end	Data number	Ancillary data	Data source	Region	Literature
C1	American Samoa	-14.25	-170.56	77	1975	2015	296716	N/A	TOAR-II DB	R2	
C2	Trinidad Head	41.05	-124.15	107	2002	2021	144515	N/A	TOAR-II DB	R1	
C3	Tudor Hills	32.27	-64.88	30	1988	2021	205951	N/A	TOAR-II DB	R7	
C4	Ragged Point	13.17	-59.43	45	1989	2017	121400	N/A	TOAR-II DB	R8	
C5	Minamitorishima	24.29	153.98	7	1994	2020	227252	N/A	TOAR-II DB	R1	
C6	Cape Hedo	26.87	128.25	68	2000	2021	182731	N/A	EANET, https://monitoring.eanet.asia/document/signin/index	R1	
C7	Ogasawara	27.09	142.22	212	2000	2021	175470	N/A	EANET, https://monitoring.eanet.asia/document/signin/index	R1	
C8	Kennaook-Cape Grim	-40.68	144.69	94	1981	2020	301842	N/A	CSIRO	R3	<u>Galbally et al. (2000)</u>
C9	Mace Head	53.33	-9.9	8	1988	2021	286705	N/A	TOAR-II DB	R7	
C10	Cabo Verde	16.86	-24.87	10	2006	2022	134538	CO	TOAR-II DB	R8	
C11	Cape Point	-34.35	18.49	230	2015	2021	40613	N/A	TOAR-II DB	R9	
C12	Ushuaia	-54.85	-68.31	18	1994	2022	202431	N/A	TOAR-II DB	R9	
C13	Baring Head	-41.41	174.87	85	1991	2021	211900	N/A	TOAR-II DB	R3	
C14	Mauna Loa	19.54	-155.58	3397	1957	2021	412530	N/A	TOAR-II DB	R2	
C15	Sable Island	43.93	-59.9	8	2003	2014	78813	NO, NO ₂ , NO _x	TOAR-II DB	R7	
C16	Izana	28.31	-16.5	2373	1987	2022	300331	N/A	TOAR-II DB	R7	
C17	Faial	38.61	-28.63	N/A	2007	2020	98546	NO, NO ₂ , NO _x	TOAR-II DB	R7	
C18	Cheeka Peak	48.3	-124.62	466	2006	2022	113646	CO	TOAR-II DB	R1	
C19	Bukit Kototabang	-0.2	100.32	864	2007	2021	93431	N/A	TOAR-II DB	R2	



C2 0	SanCristobal_Gal apagos	-0.9	-89.61	14	2000	2012	16477	N/A	campaign	R2	<u>Gómez Martín et al. (2016)</u>
C2 1	Isabela_Island	-0.96	-90.97	5	2010	2011	4419	NO ₂	campaign	R2	<u>Gómez Martín et al. (2016)</u>



Table 5. List of polar ground-based observations contained in the polar sites data set.

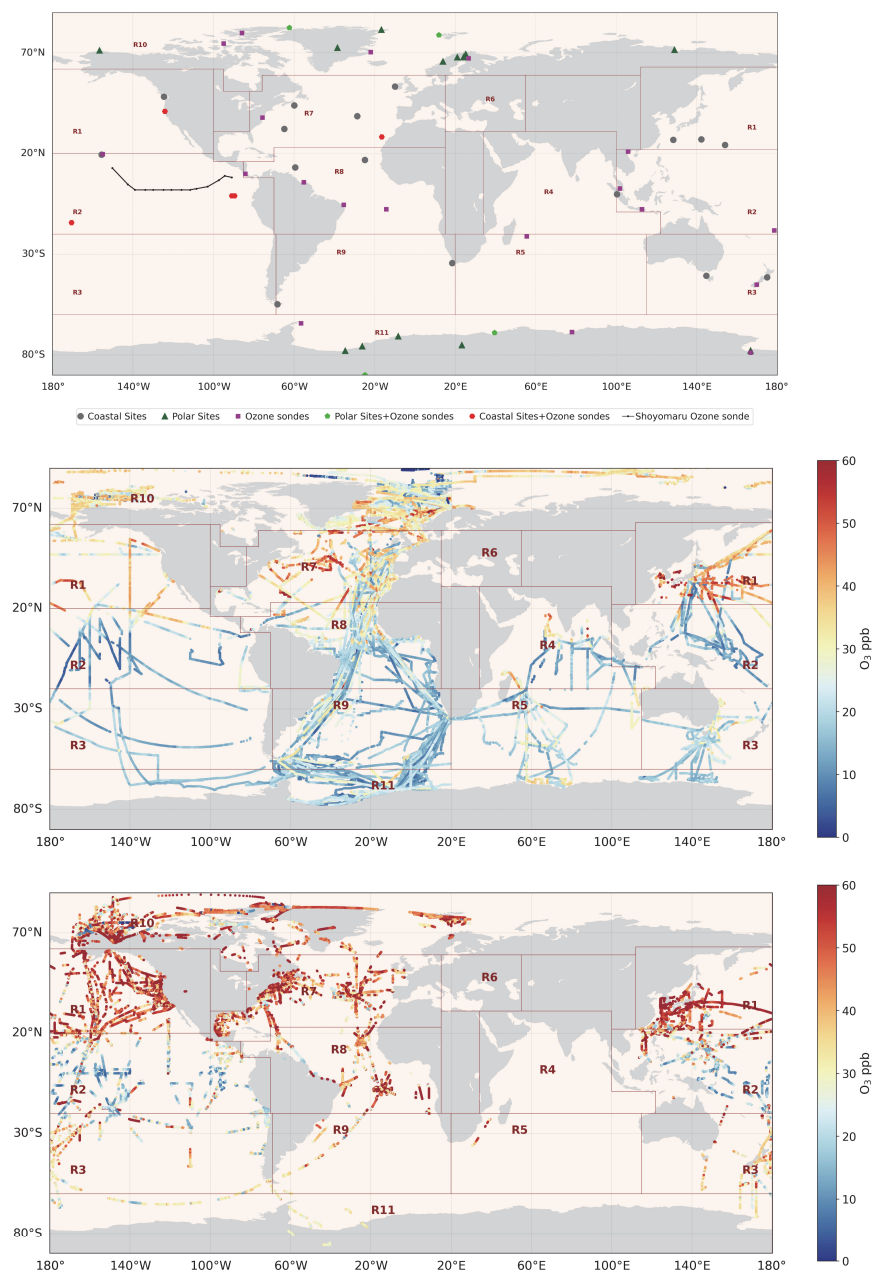
735

Label	Station	Latitude	Longitude	Altitude (m)	Year begin	Year end	Data number	Ancillary data	Data source	Region
P1	Barrow	71.32	-156.61	11	1973	2021	399426	N/A	TOAR-II DB	R10
P2	South Pole	-90.0	-24.8	2841	1975	2021	383899	N/A	TOAR-II DB	R11
P3	Syowa	-69.01	39.59	16	1997	2022	208564	N/A	TOAR-II DB	R11
P4	Alert	82.45	-62.51	210	1992	2022	228231	N/A	Canadian data site https://data-donnees.az.ec.gc.ca/data/air/monitor/national-air-pollution-surveillance-naps-program/Data-Donnees/?lang=en	R10
P5	Arrival Heights	-77.83	166.66	184	1996	2021	204240	N/A	TOAR-II DB	R11
P6	Villum	81.6	-16.67	20	2001	2021	106839	N/A	TOAR-II DB	R10
P7	Pallas	67.97	24.12	565	1995	2020	216419	NO ₂	TOAR-II DB	R10
P8	Neumayer	-70.67	-8.27	42	1995	2021	203827	N/A	TOAR-II DB	R11
P9	Zeppelin mountain	78.91	11.89	474	1989	2022	219504	CO	TOAR-II DB	R10
P10	Karasjok	69.47	25.22	333	1997	2010	109445	N/A	TOAR-II DB	R10
P11	Concordia	-75.1	23.33	3233	2006	2022	91958	N/A	TOAR-II DB	R11
P12	Halley	-75.62	-26.18	30	2007	2022	88916	N/A	TOAR-II DB	R11
P13	Esrange	67.88	21.07	475	1990	2021	267012	N/A	TOAR-II DB	R10
P14	Tiksi	71.59	128.92	8	2010	2018	51107	N/A	TOAR-II DB	R10
P15	Tustervatn	65.83	13.91	439	1989	2022	275764	N/A	TOAR-II DB	R10
P16	Summit	72.58	-38.48	3238	2000	2021	169281	N/A	TOAR-II DB	R10
P17	Belgrano	-77.87	-34.62	256	2007	2023	138284	N/A	INTA	R11



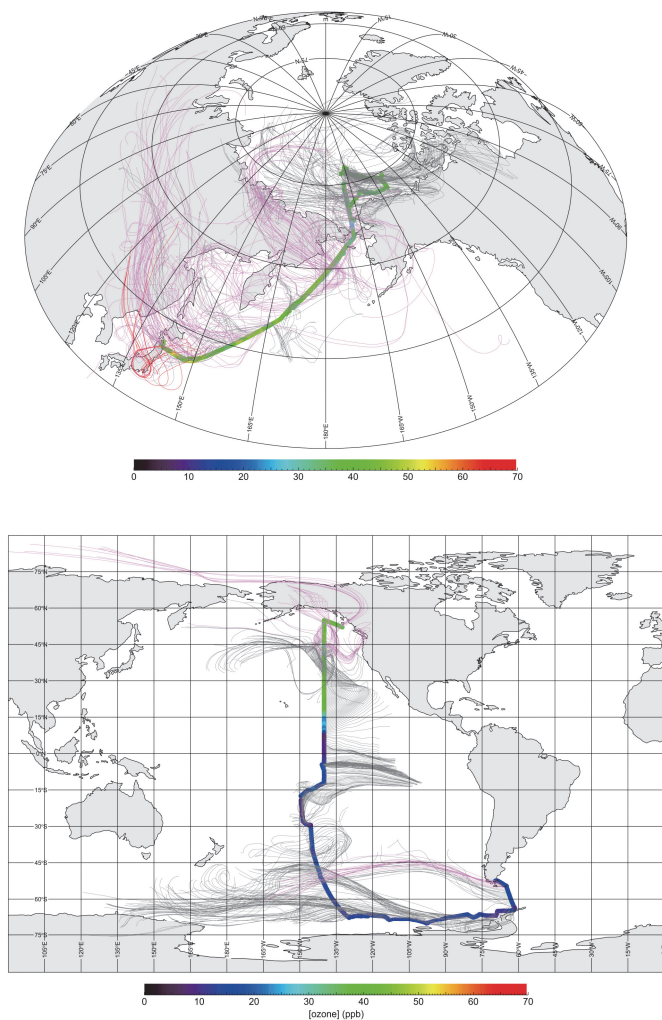
Table 6. Statistics of hourly data from the ship/buoy dataset per defined regions (R1–R11).

Regions	Number of hourly data (satisfying LCL72)	Maximum of hourly medians (ppb)	Local Time (hour) of maximum	Minimum of hourly medians (ppb)	Local Time (hour) of minimum	Average of 24 hourly medians (ppb)	Amplitude (max-min) (ppb)	Percentage amplitude (max-min)/average (%)
R1	6572	34.3	5	31.2	20	32.9	3.1	9.4
R2	9708	14.6	1	12.9	15	13.8	1.7	12.3
R3	6432	20.7	1, 4	19.5	14	20.1	1.2	5.7
R4	3446	17.3	3	14.7	16	16.2	2.6	16.0
R5	5651	20.0	8	19.2	0	19.7	0.9	4.4
R7	14777	32.5	1, 3, 4	30.5	14	31.6	2.0	6.5
R8	18818	21.3	5	19.0	15	20.0	2.3	11.3
R9	13710	16.0	4	15.0	15,16	15.4	1.0	6.5
R10	61708	27.5	11	25.8	8,13	26.2	1.7	6.5
R11	20215	16.0	0-7, 16-23	15.5	13	15.9	0.5	3.3



745

Figure 1. Locations of ozonesonde and coastal/polar ground observations (top). Overall ship/buoy (middle), and airborne with altitudes < 5000 m (bottom) ozone data after filtering for LCL \geq 72 h. Ozone levels above 60 ppb cut off for clarity.



750

Figure 2. Backward trajectories for essentially marine (grey) and land-influencing (purple) air masses during (top) the MR19-03C observations from 29 Sep 2019 to 10 Nov 2019 and (bottom) the RITS94 observations from 23 Nov 1993 to 6 Jan 1994. The red lines indicate cases where the observed O₃ mixing ratio is greater than 50 ppb.



755

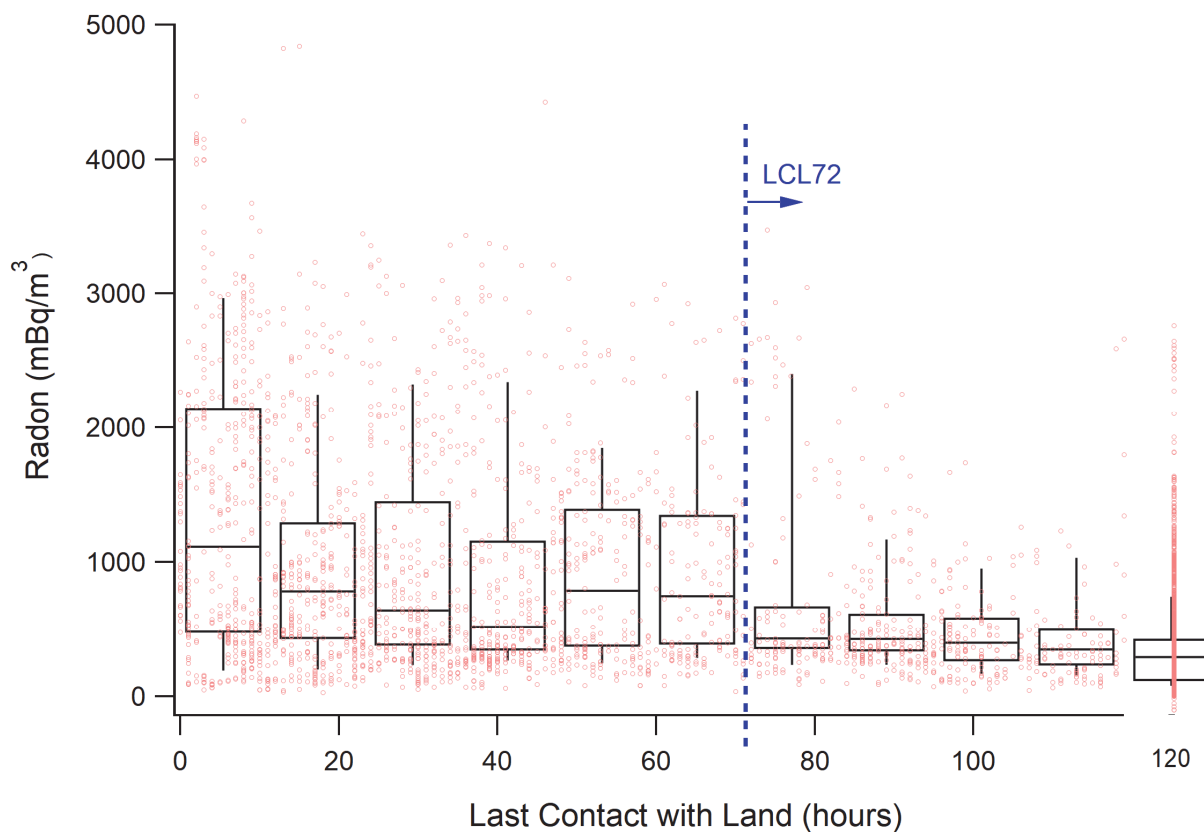
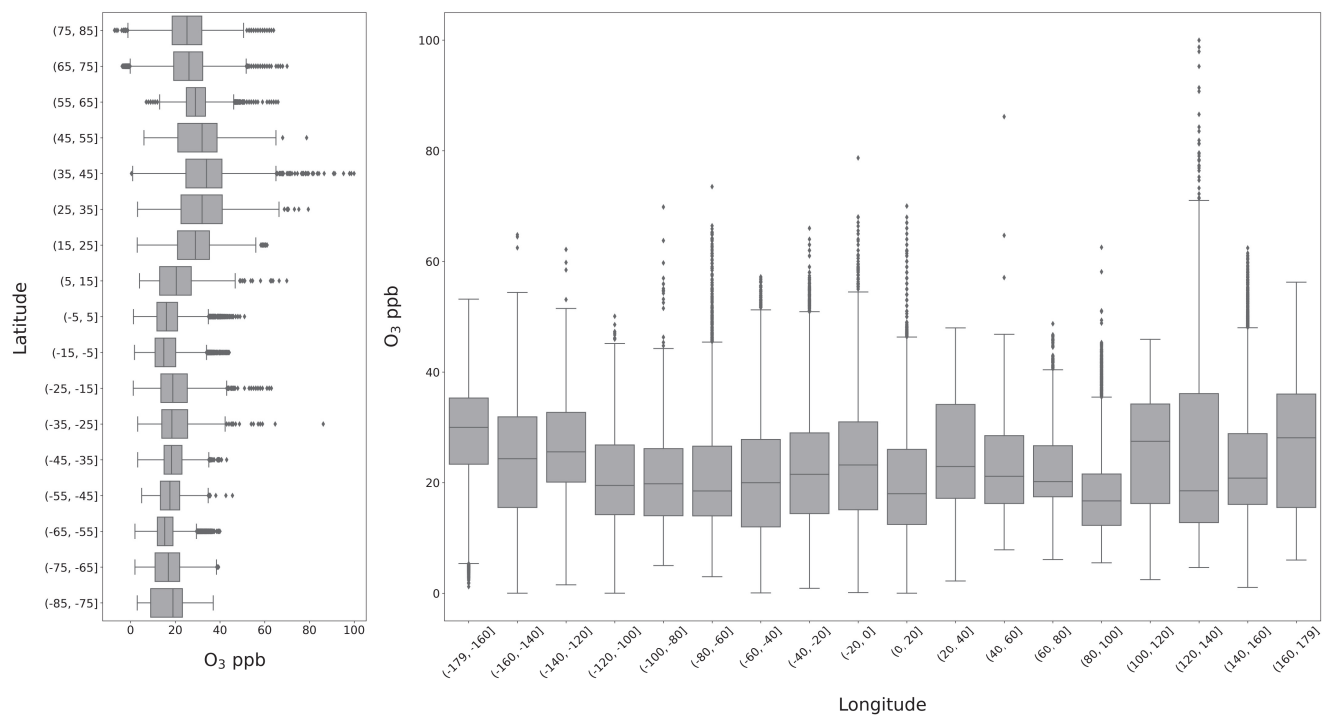


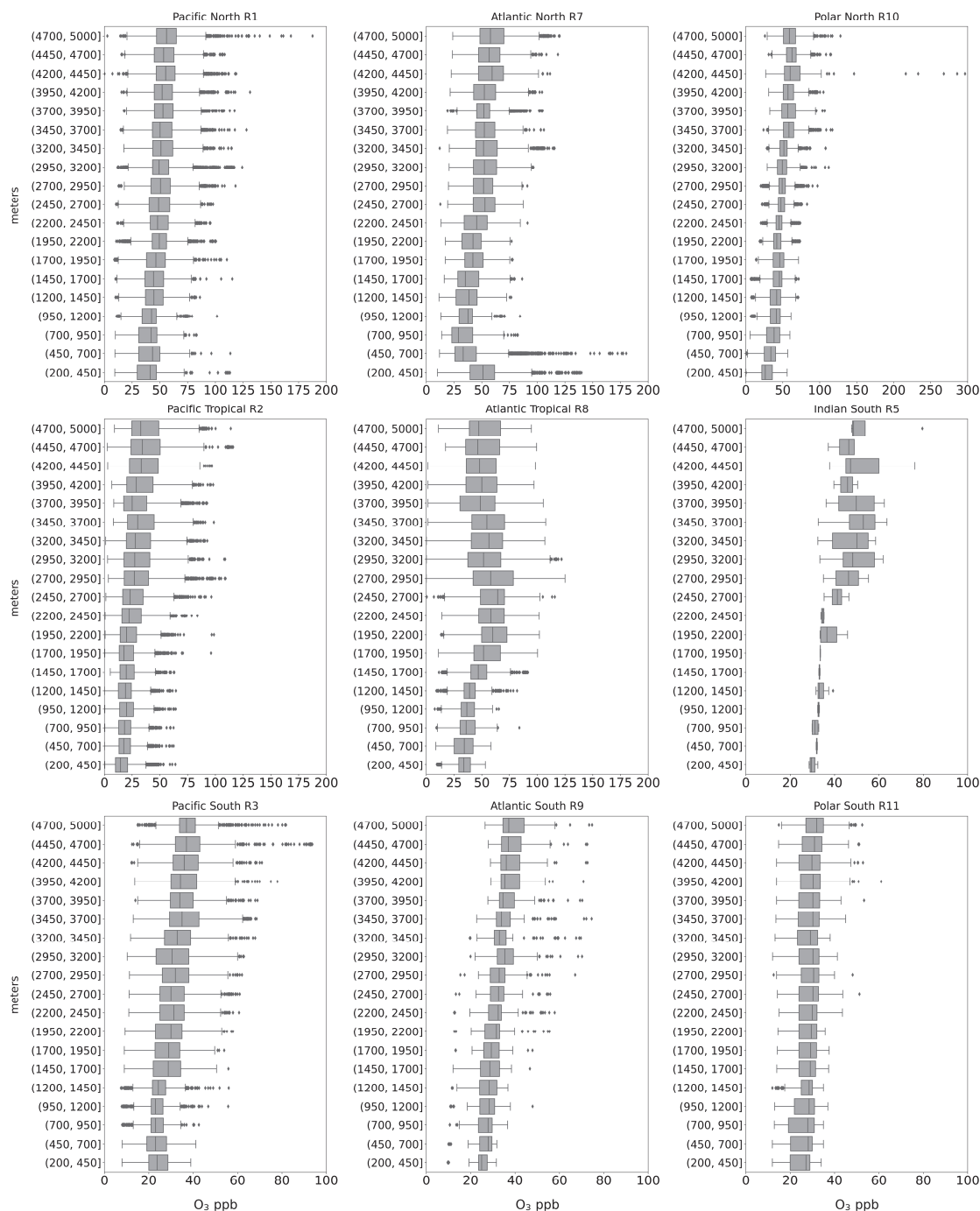
Figure 3. Decrease of Radon concentrations with Last Contact with Land from backward trajectory analysis. ACE-1, ACE-Asia, ATOMIC, ICEALOT, NAAMES1-4, and WACS data were used in combination. Radon data by NOAA PMEL. The blue dotted line indicates the adopted LCL72 criterion. Boxes and whiskers represent 10, 25, 50, 75 and 90 percentiles.

760



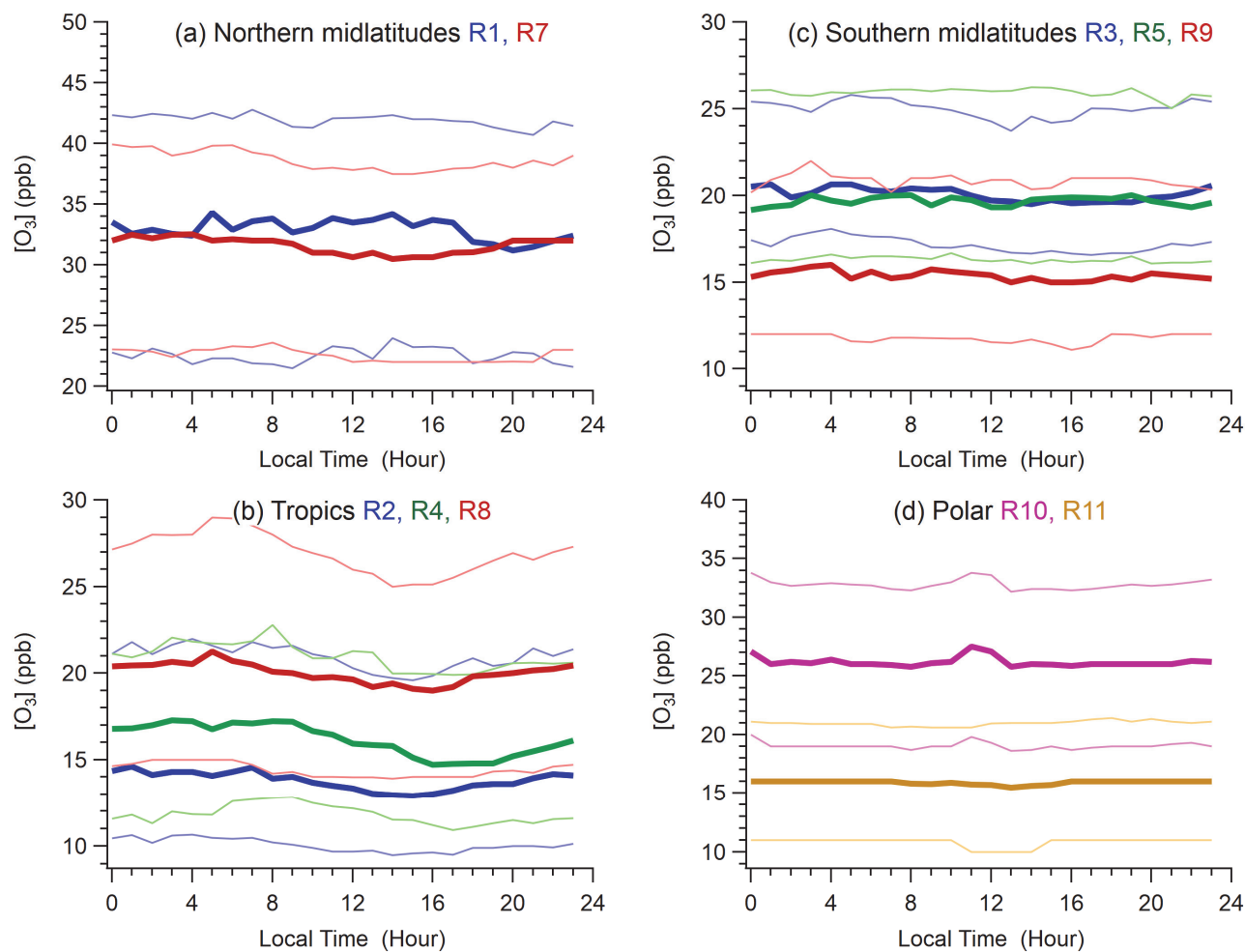
765

Figure 4. Latitudinal and longitudinal transect of the ship/buoy datasets, after filtering for LCL \geq 72 h.



770

Figure 5. Vertical profiles of ozone concentrations by regions, after filtering for LCL72.



775 **Figure 6.** Hourly median (thick lines) and interquartile levels (thin lines) and their diurnal variation by regions. (a) R1 and R7
(Pacific and Atlantic northern midlatitudes), (b) R2, R4, and R8 (Pacific, Indian, and Atlantic low latitudes), (c) R3, R5, and
R9 (Pacific, Indian, and Atlantic southern midlatitudes), and (d) R10 and R11 (Polar, i.e., Arctic and Antarctic regions). The
blue, green, and red line colors correspond to the Pacific, Indian, and Atlantic Oceans.

780



785

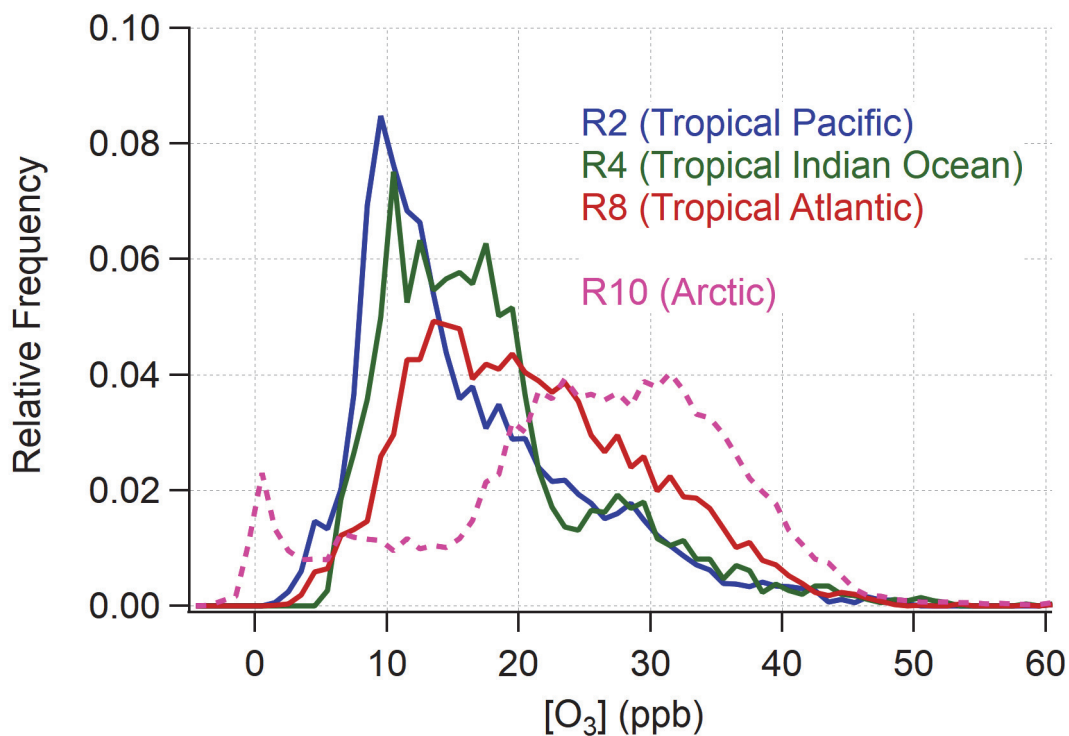
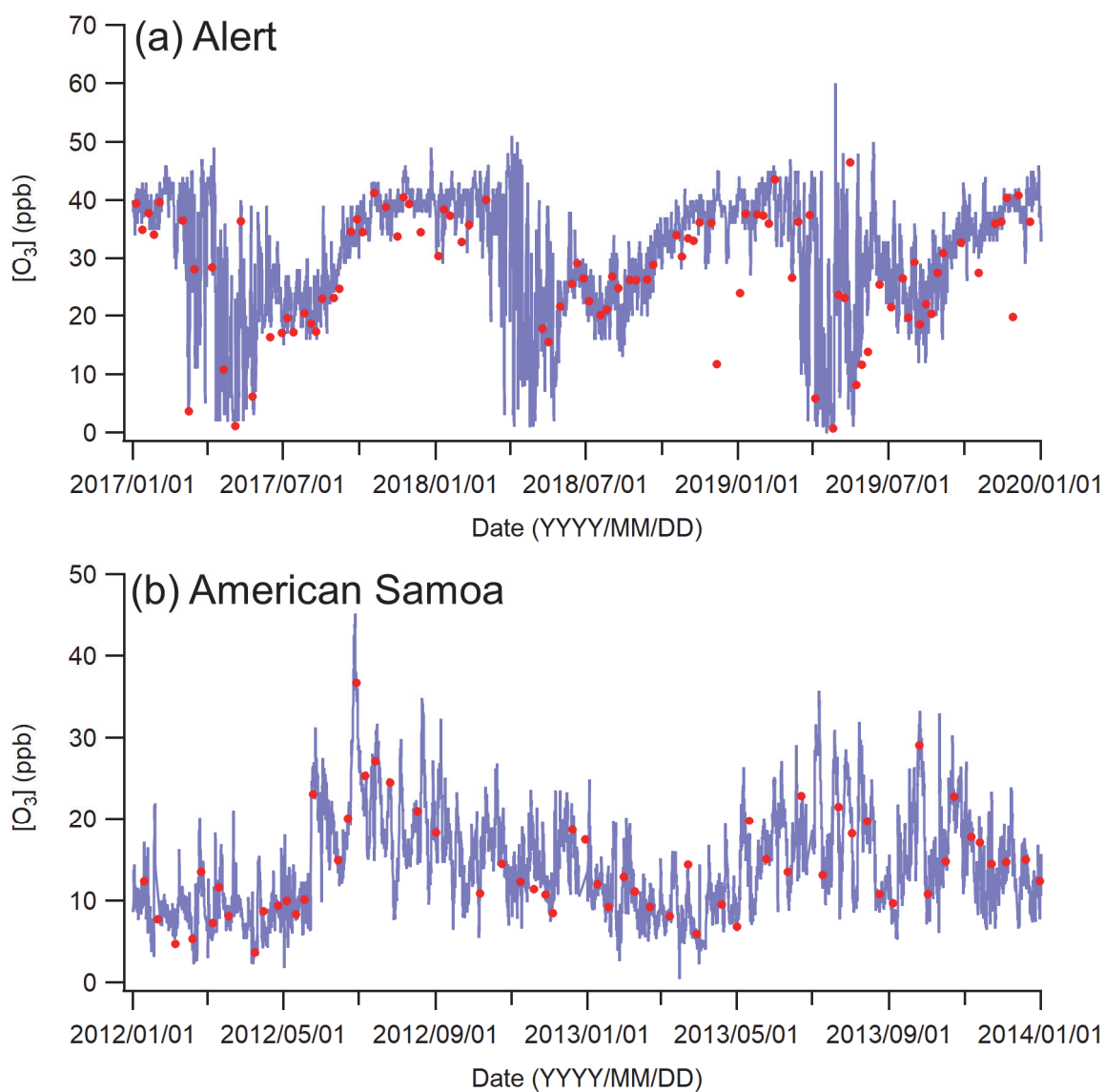


Figure 7. Frequency of observed O₃ concentrations in 1 ppb bins computed for ship and buoy observations with LCL ≥ 72 h for tropical regions (Pacific Ocean R2, Indian Ocean R4, and Atlantic Ocean R8) contrasted with the Arctic (R10).



790



795

Figure 8. O₃ concentrations from surface observations (blue) and the lowest layer of ozonesonde observations (red, ~200 m altitude) at (a) Alert (top panel) and (b) American Samoa (bottom panel).